**Atmospheric
Chemistry
and Physics**

Oxidative capacity of the Mexico City atmosphere – Part 1: A radical source perspective

R. Volkamer[1,2,3], **P. Sheehy**[1,4], **L. T. Molina**[1,4], **and M. J. Molina**[1,2]

[1]Department of Earth, Atmospheric and Planetary Sciences, Massachussetts Institute of Technology, Cambridge, MA, USA
[2]Department of Chemistry and Biochemistry, University of California, San Diego, La Jolla, CA, USA
[3]Department of Chemistry and Biochemistry and CIRES, University of Colorado at Boulder, Boulder, CO, USA
[4]Molina Center for Energy and the Environment (MCE[2]), La Jolla, CA, USA

Abstract. A detailed analysis of OH, HO_2 and RO_2 radical sources is presented for the near field photochemical regime inside the Mexico City Metropolitan Area (MCMA). During spring of 2003 (MCMA-2003 field campaign) an extensive set of measurements was collected to quantify time-resolved RO_x (sum of OH, HO_2, RO_2) radical production rates from day- and nighttime radical sources. The Master Chemical Mechanism (MCMv3.1) was constrained by measurements of (1) concentration time-profiles of photosensitive radical precursors, i.e., nitrous acid (HONO), formaldehyde (HCHO), ozone (O_3), glyoxal (CHOCHO), and other oxygenated volatile organic compounds (OVOCs); (2) respective photolysis-frequencies (J-values); (3) concentration time-profiles of alkanes, alkenes, and aromatic VOCs (103 compound are treated) and oxidants, i.e., OH- and NO_3 radicals, O_3; and (4) NO, NO_2, meteorological and other parameters. The RO_x production rate was calculated directly from these observations; the MCM was used to estimate further RO_x production from unconstrained sources, and express overall RO_x production as OH-equivalents (i.e., taking into account the propagation efficiencies of RO_2 and HO_2 radicals into OH radicals).

Daytime radical production is found to be about 10–25 times higher than at night; it does not track the abundance of sunlight. 12-h average daytime contributions of individual sources are: Oxygenated VOC other than HCHO about 33%;
HCHO and O_3 photolysis each about 20%; O_3/alkene reactions and HONO photolysis each about 12%, other sources <3%. Nitryl chloride photolysis could potentially contribute ~15% additional radicals, while NO_2^* + water makes – if any – a very small contribution (~2%). The peak radical production of ~7.5 10^7 molec cm^{-3} s^{-1} is found already at 10:00 a.m., i.e., more than 2.5 h before solar noon. O_3/alkene reactions are indirectly responsible for ~33% of these radicals. Our measurements and analysis comprise a database that enables testing of the representation of radical sources and radical chain reactions in photochemical models.

Since the photochemical processing of pollutants in the MCMA is radical limited, our analysis identifies the drivers for ozone and SOA formation. We conclude that reductions in VOC emissions provide an efficient opportunity to reduce peak concentrations of these secondary pollutants, because (1) about 70% of radical production is linked to VOC precursors; (2) lowering the VOC/NO_x ratio has the further benefit of reducing the radical re-cycling efficiency from radical chain reactions (chemical amplification of radical sources); (3) a positive feedback is identified: lowering the rate of radical production from organic precursors also reduces that from inorganic precursors, like ozone, as pollution export from the MCMA caps the amount of ozone that accumulates at a lower rate inside the MCMA. Continued VOC reductions will in the future result in decreasing peak concentrations of ozone and SOA in the MCMA.

Correspondence to: R. Volkamer
(rainer.volkamer@colorado.edu)

1   Introduction

Air pollution is an increasingly important concern in the public health debate (Health Effects Institute, 2000). In Mexico City the number of deaths associated with anthropogenic air pollution is comparable to that from car accidents (Molina and Molina, 2002). Ozone (O_3) and fine particulate matter ($PM_{2.5}$, particles with a diameter smaller than 2.5 micrometers) are integral components of photochemical smog. There is no evidence of a "safe" threshold concentration for O_3 or $PM_{2.5}$ related health effects. O_3 is known to cause inflammation in the respiratory tract, reduce respiratory capacity for some people, and increase hospitalization rates related to asthma and other respiratory ailments. More recently, systematic evidence has been presented supporting premature mortality in relation to short-term O_3 exposure following episodes of photochemical smog in the US (Bell et al., 2004) and Asia (PAPA, 2004). Downwind of urban areas, photochemical O_3 leads to reduced tree-growth (Gregg et al., 2003), has adverse effects on agriculture (Fuhrer and Booker, 2003), and contributes to global warming (IPCC, 2007). Short-term exposures to high levels of $PM_{2.5}$ (e.g., $500\,\mu g/m^3$) caused premature mortality during the London killer smog episode in 1952 (Davis et al., 2002); more recent studies in the US, Europe, Asia, and South America have further found association of long-term exposures to $PM_{2.5}$ with premature mortality at much lower levels ($<50\,\mu g/m^3$) (Health Effects Institute, 2000; Pope et al., 2002). Recent progress toward identifying biological mechanisms for these effects point to the role of transition metals and pro-oxidative hydrocarbons associated with fine particulate matter (Nel, 2005). Enhanced light absorption by aerosols affects climate (Ramanathan et al., 2001) with implications for atmospheric stability and vertical air exchange, precipitation patterns, and the amount of radiation reaching the ground.

Photochemical smog is largely formed as the result of the chemical transformations of primary emissions to the atmosphere. It has long been understood that O_3 is not directly emitted, but forms in the atmosphere as a result of hydrocarbon/NO_x/sunlight photochemistry (Haagen-Smit et al., 1951). On the other hand, it has only recently been recognized that in Mexico City and other urban areas – despite the abundance of emission sources – gas-to-particle conversion processes are responsible for about 60–80% of $PM_{2.5}$ mass; secondary organic aerosol (SOA) originating from the gas-phase oxidation of hydrocarbons is a major component of $PM_{2.5}$ (Salcedo et al., 2006; Volkamer et al., 2006; Zhang et al., 2007). Free radical (i.e., OH and NO_3), O_3, and photolysis reactions initiate the oxidation of hydrocarbons in the gas-phase, and possibly modify aerosol surfaces. The design of effective policy strategies to reduce the impact of air pollution on human health, ecosystem and climate requires understanding the sources and sinks of these radicals. Modeling studies (Ruiz-Suarez et al., 1993; West et al., 2004; Lei et al., 2007, 2008) and experimental observations (Arriaga-Colina et al., 2004) suggest that the photochemical processing of pollutants in the MCMA is either VOC limited or suppressed by high NO_x levels; indeed both of these chemical regimes may apply at different times (Lei et al., 2007, 2008; Stephens et al., 2008). In either case, the photochemical processing of pollutants is radical limited. This suggests that a more detailed understanding of radical sources can identify mechanisms to efficiently slow down photochemical smog formation, including O_3 and SOA formation in the MCMA.

The chemical mechanisms that underlie atmospheric model predictions of ozone (and fine $PM_{2.5}$) are simplified representations of a rather complex chemistry of the urban atmosphere. The result of such "chemical lumping" is that atmospheric models become heavily parameterized when addressing a specific target question (e.g., predicting ozone). However, the optimal parameterization is different for different atmospheric conditions (e.g., VOC/NO_x ratio); once a model has been optimized, it remains a challenge to predict ozone if atmospheric conditions change. There is a hidden uncertainty in "lumped" chemistry modules that can account for errors as large as 10–60% in the predicted ozone as atmospheric conditions change (Carter et al., 2005; Bloss et al., 2005a, b; Stockwell et al., 2008). This chemical uncertainty is in addition to those caused by uncertainties in meteorology and emissions. It is comparable in magnitude, but often neglected for consideration. This paper series investigates this "hidden" uncertainty directly by means of a detailed chemical model that has a minimum amount of chemical lumping. The model explicitly represents the formation and sink reactions of OH, HO_2, and RO_2 radicals (in sum termed RO_x radicals), and thus does not suffer from changing experimental conditions. Part 1 of the series focuses on the production of RO_x radicals from the reaction of closed shell molecules with sunlight (i.e., HONO, HCHO, O_3, glyoxal, numerous other oxygenated VOC (OVOC)), and the dark reaction of alkenes with O_3 and NO_3 radicals. Most of these radical sources are constrained by observations. In Part 2 Sheehy et al. (2010) the experimental radical production rates from this work are combined with observations of HO_x radicals (Shirley et al., 2006) to directly quantify (1) the amplification of radical sources from chemical radical chain reactions, and (2) to assess our current capability to predict radical chain reactions that largely determine the oxidation capacity. Since these radicals have lifetimes on the order of few milliseconds to seconds, the comparison of measured and predicted radical concentrations systematically minimizes uncertainty from air movements and emissions, and isolates the uncertainty inherent in our limited understanding of oxidative chemistry.

2   Experimental

As part of the MCMA-2003 field campaign, time-resolved production of HO_x radicals released from the decomposition of closed shell molecules were quantified. A comprehensive

set of instrumentation to characterize radical precursor concentrations, their respective photolysis frequencies, and oxidants (OH, O_3, NO_3) was based at a supersite located at the Centro Nacional de Investigación y Capacitación Ambiental (CENICA) in the central-southern part of the MCMA. An overview of typical pollutant concentrations at the CENICA site is compiled in Molina et al. (2007); campaign median concentrations were 86 ppb NO_x during morning rush hour, 20 ppb NO_x during afternoons, median peak concentrations of 115 ppb O_3, 0.4 ppt OH, and 40 ppt HO_2 shortly after noon, 120 s^{-1} OH-reactivity (morning rush hour). Of the calculated contributions to the OH reactivity, 12% was due to NO_x, 7% to CO, 4% to HCHO and 72% to VOCs (Shirley et al., 2006). The instruments that measured radical precursor molecules are described in the following sections; more than 75% of the overall rate of radical production is constrained by measurements here. A complete list of measurements used to constrain the MCM model as given in the Supplementary Material of Sheehy et al. (2010).

2.1 Measurement techniques

The radical precursor molecules HONO, HCHO, O_3, and CHOCHO were measured by Long-Path Differential Optical Absorption Spectroscopy (LP-DOAS), acetaldehyde and acetone were measured by PTR-MS (Jobson et al., 2010), and the respective photolysis frequencies for these molecules were measured by spectroradiometry as described below. Alkenes and other hydrocarbons were measured by a Fast Isoprene Sensor (FIS) and VOC canister samples (Velasco et al., 2007), open path DOAS and FTIR (see below), and PTR-MS (Jobson et al., 2010).

2.1.1 Long-Path Differential Optical Absorption Spectrometry (LP-DOAS)

Two LP-DOAS instruments were deployed on the rooftop of the CENICA building. DOAS uses unique specific narrow-band (<5 nm) absorption structures in the visible spectral range to separate trace gas absorptions from broadband molecule and aerosol extinction in the open atmosphere (Platt, 1994). The DOAS#1 light path was directed towards an antenna tower in a south-easterly direction at an average height of 16 m with a 430 m path length (total 860 m). DOAS#2 faced an array of retro reflectors at Museo Fuego Nuevo (Cerro de la Estrella) resulting in a total light-path of 4420 m and average 70 m above ground. Atmospheric spectra were recorded by sequentially projecting 40-nm (DOAS#1) and 80-nm (DOAS#2) wide wavelength intervals centered around 260 nm, 318 nm, 357 nm, 427 nm and 642 nm onto the 1024-element linear photodiode array detector; background spectra recorded within a few minutes were subtracted to correct for stray-light from the atmosphere. The average time-resolution for a full cycle of spectra ranged between 30 s–4 min (DOAS#1), and 2–15 min (DOAS#2), de-

pending on the light extinction due to ozone (DOAS#1), NO_2 and aerosols (DOAS#1 and DOAS#2).

DOAS#1 measured O_3, NO_2, SO_2, HONO, HCHO, benzene, toluene, m-xylene, p-xylene, mono-substituted alkyl-benzenes (C_2 and higher), phenol, p-cresol, and benzaldehyde by observing unique specific ro-vibronic absorption structures distributed over several hundred wavelength channels simultaneously. Naphthalene and styrene were also measured for the first time with DOAS in the atmosphere (Volkamer et al., 2004). Reference spectra of aromatic compounds were recorded by introducing quartz-cuvettes filled with vapor into the light beam, and these spectra were calibrated by using absorption cross-section spectra taken from the literature (Etzkorn et al., 1999). Absorptions of atmospheric oxygen were eliminated using the interpolation approach of Volkamer et al. (1998). In brief, saturation of molecular absorption lines of oxygen in the Herzberg I-III bands were modeled in high-resolution using line parameters from Fally et al. (2000), Jenouvrier et al. (1999) and Merienne et al. (2000, 2001), and oxygen column densities of 3.7×10^{17} molecules cm^{-2} and 4.1×10^{17} molecules cm^{-2} to bracket the effect of density variations on oxygen column densities. The collision induced absorption of oxygen in the Wulf bands was fitted using the literature spectra from Bernath et al. (1998). For ozone, temperature dependent absorption cross-sections (Bass and Paur, 1981) for 293 K and 313 K were convoluted to match the spectral resolution of the instruments, and fitted simultaneously with other trace-gas reference spectra and a fifth order polynomial high-pass filter to account for broadband molecule and aerosol extinction using non-linear least squares fitting routines (Stutz et al., 1996; Fayt et al., 2001). The mean detection limits of species measured by DOAS#1 were: 1.3 ppbv (O_3), 1.5 ppbv (NO_2), 0.26 ppbv (SO_2), 0.5 ppbv (HONO), 5 ppbv (HCHO), 1 ppbv (benzene, toluene, m-xylene), 0.3 ppbv (p-xylene), 1.8 ppbv (ethylbenzene-equivalents), 0.5 ppbv (styrene), 0.06 ppbv (phenol, p-cresol), 0.2 ppbv (benzaldehyde), and 0.08 ppbv (naphthalene).

From the spectra collected by DOAS#2, HCHO and ozone were evaluated in the wavelength range between 324 to 358 nm using non-linear least squares fitting of HCHO, HONO, NO_2, two O_3 references at 293 K and 313 K, SO_2, and a 5th order polynomial high pass filter. HONO was retrieved in the wavelength range between 321 to 372 nm using non-linear least squares fitting of HONO, HCHO, NO_2, two O_3 references at 293 K and 313 K, SO_2, and a 9th order polynomial high-pass filter. CHOCHO was retrieved from evaluating the spectral range between 420 and 465 nm, using non-linear least squares fitting of CHOCHO, NO_2, O_4, H_2O, two lamp-reference spectra, and a 5th order polynomial high-pass filter; these data are discussed in more detail by Volkamer et al. (2005a). In addition, NO_3 radicals were detected at nighttime. Reference spectra were calculated from high-resolution absorption cross-section spectra, which were degraded to our instrument resolution (ca. 0.4 nm

Table 1. The percentage contributions of individual sources to OH_{new} (bold numbers). Individual molecules are differentiated by their source (italic numbers, add up to 100% for any given source); for "other OVOC" sources for OH_{new} from HO_2 and RO_2 radicals are differentiated (italic numbers), and differentiated by molecular functional groups (small roman numbers, add up to 100% in the HO_2 and RO_2 sub categories).

		contribution to ΣOH_{new}							
		03:00	07:00	09:00	11:00	13:00	15:00	20:00	06:00–18:00 (avg)	20:00–04:00 (avg)
Measured	**HONO**	**–**	**42.1**	**21.8**	**7.4**	**3.9**	**1.1**	**–**	**11.8**	**–**
	PSS[a]	*–*	*53–98*	*91–99*	*45–86*	*53–92*	*50–94*	*–*	*80–90*	*–*
	Dark + other[a]	*–*	*≤47*	*≤9*	*≤55*	*≤47*	*≤50*	*–*	*≤20*	*–*
	O₃	**–**	**–**	**4.0**	**21.7**	**36.4**	**29.7**	**–**	**19.2**	**–**
	HCHO	**–**	**4.4**	**20.3**	**23.5**	**20.7**	**18.3**	**–**	**19.4**	**–**
	Primary[b,c]	*–*	*60.5*	*40.0*	*11.9*	*0.1*	*6.2*	*–*	*28.6*	*–*
	Other[b,c]	*–*	*39.5*	*60.0*	*88.1*	*99.9*	*93.8*	*–*	*71.4*	*–*
	CH₃CHO	**–**	**0.1**	**0.5**	**0.8**	**1.0**	**1.4**	**–**	**0.8**	**–**
	CHOCHO	**–**	**0.1**	**0.7**	**1.0**	**1.1**	**0.8**	**–**	**0.8**	**–**
	CH₃COCH₃	**–**	**0.1**	**0.2**	**0.3**	**0.4**	**0.4**	**–**	**0.3**	**–**
	O₃+alkenes	**81.9**	**22.6**	**16.6**	**9.2**	**4.1**	**10.5**	**78.7**	**12.0**	**84.7**
	→OH[c]	*55.3*	*48.2*	*50.6*	*52.7*	*53.3*	*53.6*	*55.1*	*51.9*	*53.2*
	→HO₂[c]	*8.2*	*6.6*	*9.0*	*12.1*	*12.5*	*11.7*	*9.6*	*10.2*	*8.1*
	→ RO₂[c]	*36.5*	*45.2*	*40.4*	*35.2*	*34.2*	*34.7*	*35.4*	*37.9*	*38.7*
	NO₂*	**–**	**2.1**	**4.3**	**1.6**	**0.8**	**1.3**	**–**	**2.1**	**–**
Modeled	**ROOH**	**–**	**1.0**	**1.7**	**1.2**	**1.6**	**2.5**	**–**	**0.9**	**–**
	→OH	*–*	*4.3*	*4.9*	*23.3*	*62.6*	*70.6*	*–*	*62.6*	*–*
	→RO₂	*–*	*95.7*	*95.1*	*76.7*	*37.4*	*29.4*	*–*	*37.4*	*–*
	other OVOC	**–**	**25.1**	**28.9**	**31.0**	**27.6**	**29.6**	**–**	**30.3**	**–**
	→HO₂[c]	*–*	*51.1*	*56.1*	*60.3*	*60.7*	*61.1*	*–*	*57.6*	*–*
	carbonyls	–	83.8	69.7	68.7	67.9	70.6	–	69.7	–
	RCHO	–	2.7	10.6	18.8	22.5	16.8	–	16.4	–
	EPOX	–	12.2	17.5	9.8	7.2	10.8	–	11.6	–
	Ketones	–	–	0.2	0.5	0.8	0.6	–	0.5	–
	MISC	–	1.3	2.1	2.5	1.4	1.0	–	1.7	–
	→RO₂[c]	*–*	*47.8*	*42.2*	*38.8*	*38.7*	*38.2*	*–*	*42.4*	*–*
	carbonyls	–	94.2	85.7	81.3	80.5	84.8	–	83.5	–
	RCHO	–	1.6	7.2	11.8	12.1	8.4	–	9.7	–
	Ketones	–	0.3	1.7	3.7	5.2	4.4	–	3.4	–
	Misc	–	2.3	1.6	1.0	0.7	0.5	–	1.0	–
	NO₃+VOC	**18.1**	**0.2**	**1.1**	**2.1**	**1.9**	**3.8**	**21.3**	**2.2**	**15.3**
	Sum (%)	100.0	97.8	100.0	99.8	99.5	99.5	100.0	99.9	100.0
	ΣOH_{new} (ppb h⁻¹)	0.48	1.95	10.53	12.68	8.55	4.11	0.77	6.45	0.48

[a] PSS: photostationary state HONO; dark+other: unaccounted HONO sources. Numbers indicate relative contributions to ΣOH_{new} from HONO; [b] Primary: emission-related HCHO; other: photochemical and background HCHO (Garcia et al., 2006); [c] Numbers indicate relative contributions to ΣOH_{new} for a specific sub category of sources.

FWHM), and fitted using the Windoas and MFC software packages (Gomer et al., 1993; Fayt and van Roozendael, 2001). The trace-gas concentrations reported here rely on the following calibrations, with values in parentheses indicating mean detection limits for species measured by DOAS#2: HONO (190 pptv) (Stutz et al., 2000), CHOCHO (150 pptv) (Volkamer et al., 2005b), NO_3 (5 pptv) (Sander et al., 2006), O_3 (DOAS#1: 1.3 ppbv; DOAS#2: 5 ppbv) (Bass and Paur, 1981), and SO_2 (150 pptv) (Vandaele et al., 1994). For HCHO (1 ppbv) the cross-section by Cantrell et al. (1990) was used for spectra evaluation; the concentrations were multiplied by 1.22 to reflect the results from cross-calibration of ultraviolet and infrared spectral parameters of HCHO (Volkamer et al., 2005[1]). For NO_2 (430 pptv), reference spectra were recorded by placing a 2-cm long quartz-cuvette

---

[1] Volkamer et al., 2005, CP26 at http://www.colorado.edu/chemistry/volkamer/publications/index.html

into the light beam, which was filled previously with a mixture of approximately 1% NO_2/N_2 to atmospheric pressure. The $HONO/NO_2$ ratio was determined from simultaneous fitting of resolution-adjusted literature cross-sections and any HONO contamination of the cuvette was corrected by subtracting an appropriately scaled HONO spectrum from the cuvette spectrum. This approach eliminates the possibility of HONO contaminated NO_2 reference spectra; we successfully used it in cross-comparisons of the DOAS and LOPAP techniques (Kleffmann et al., 2006). NO_2 concentrations were scaled to match the average of various NO_2 reference spectra as determined by Orphal (2003). Trace-gas concentrations that were evaluated in different spectral ranges (HONO, NO_2, HCHO and O_3) were found to be independent of the spectral range used for evaluation (within error limits).

2.1.2 Proton-Transfer-Reaction Mass-Spectrometry (PTR-MS)

Acetaldehyde (CH_3CHO) and acetone (CH_3COCH_3) were measured by a PTR-MS (Jobson et al., 2010), which was co-located with the DOAS instruments at the CENICA rooftop, about 16 m above the ground. The PTR-MS sensitivity was determined with a multi-component compressed gas standard from Apel-Reimer Environmental (Denver, USA) containing acetaldehyde and acetone, among other hydrocarbons. The standard had a stated accuracy of $\pm 5\%$ for oxygenated species, better than 5% for hydrocarbons, and multipoint calibrations were performed every couple of days. Additional measurements of alkenes by a Fast Isoprene Sensor, supplemented by gas-chromatography (GC-FID) analysis of canister samples are described in detail elsewhere (Velasco et al., 2007).

2.1.3 Spectroradiometry

Photolysis frequencies of HONO (J_{HONO}), HCHO (J_{HCHO}), CH_3CHO (J_{CH_3CHO}), O_3 (J_{O_3}), CHOCHO (J_{CHOCHO}), CH_3COCH_3 ($J_{CH_3COCH_3}$) and other trace gases were measured by spectroradiometry. The spectroradiometer was mounted on top of the measurement cabin with a clear field of view and measured solar actinic flux spectra from 280 nm to 450 nm with a spectral band pass of 1 nm. The step width was set to 2 nm below 320 nm, and 5 nm above. The radiation from the upper hemisphere was collected by a diffuser-optic with almost uniform sensitivity for all angles of incidence within a solid angle of 2π sr. A double monochromator (Bentham DMc 150) equipped with a tunable grating (2400 grooves/mm) was used for wavelength dispersion and a photomultiplier for photon detection. The actinic flux calibration of the spectroradiometer was performed before and after the campaign at the Forschungszentrum Juelich in Germany using certified irradiance standards as described in Kraus et al. (2000). Unless otherwise noted, the ab-
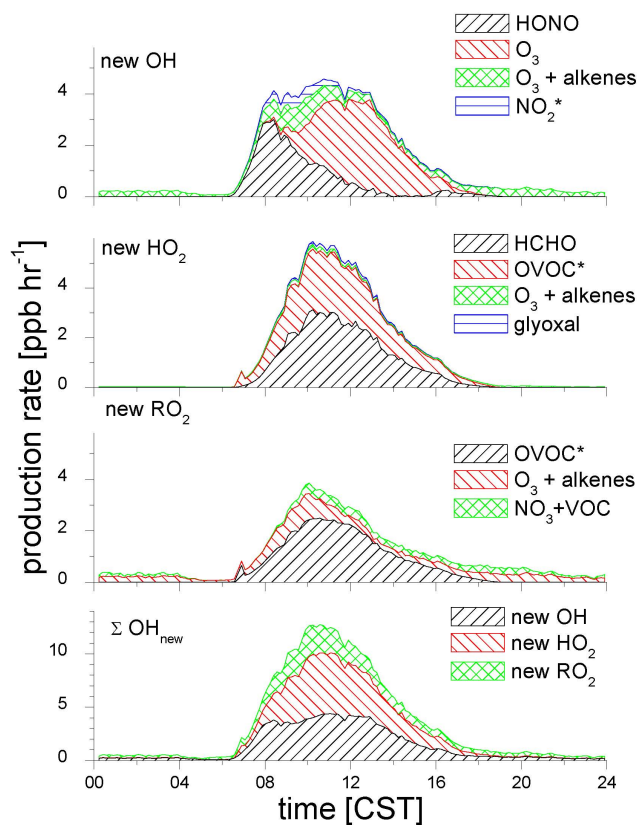

Fig. 1. Diurnal profiles of new RO_x radical formation from different sources. The categories marked with a star (*) indicate that the reactants are not constrained by measurements. The bottom graph shows the contribution of each RO_x species to ΣOH_{new}, accounting for their respective conversion factors.

sorption cross-sections used to calculate photolysis frequencies were the same as described above; for O_3, the cross-section at 295 K was employed; for HONO the current cross-section recommendation (Sander et al., 2006) was multiplied by 1.43 in order to match recent absolute measurements of J_{HONO} (Wall et al., 2006); for CH_3CHO and CH_3COCH_3 the spectrum and quantum yield data for radical producing channels were taken from Sander et al. (2006). Resultant J-values were multiplied by 1.08 (surface albedo) to account for the upwelling portion of the photon actinic flux. The overall uncertainties for the photolysis channels are 25% for ($O_3 \rightarrow O^1D$, CHOCHO→radicals), and 15% for (HONO→OH, HCHO, CH_3CHO, CH_3COCH_3 →radicals).

2.2 Radical production rate calculations

A flexible-top photochemical box model was used to calculate the radical production rates from experimentally constrained sources, and to estimate sources that were not constrained by observations. The model employs the Master Chemical Mechanism (MCM, v3.1), which is based on the

protocols developed by Saunders et al. (2003) and Jenkin et al. (2003), and has recently been updated for aromatic oxidation schemes (Bloss et al., 2005a, b). MCM, a near-explicit mechanism comprising 135 VOCs and more than 13 500 reactions, is ideally suited to test RO_x radical production because it contains limited chemical lumping. This enables (1) accounting of individual radical production and loss pathways; and (2) expression of RO_x radical production rates in terms of equivalent OH radical production rates as defined by Eq. (1):

$$\Sigma OH_{new} = P(OH) + \gamma_{HO_2} \cdot P(HO_2) + \gamma_{RO_2} \cdot \gamma_{RO} \cdot P(RO_2) \quad (1)$$

where P-values represent the rate of production of OH, HO_2 and RO_2 radicals from closed shell molecules, and gamma values represent the efficiency to propagate RO_2 and HO_2 radicals into OH radicals; γ_{HO_2}, γ_{RO_2}, and γ_{RO} are defined in Eqs. (6–8) in Sheehy et al. (2010), and are calculated by the MCM as a function of changing experimental conditions, i.e., NO, NO_3, HO_2, RO_2 concentrations, and VOC speciation.

The box-model was constrained by median time-profiles of the above radical precursor concentrations, J-values, oxidant concentrations (OH, HO_2, O_3, NO_3), and concentrations of radical sinks, i.e., 103 VOCs, NO, NO_2, SO_2, CO (Sheehy et al., 2010, Supplementary Information). The OH reactivity of the constrained model reproduced well the diurnal variations of OH-reactivity observations (Shirley et al., 2006), and were generally somewhat lower (see Part 2). The loss mechanisms of secondary species formed via the oxidation of hydrocarbons include reaction with OH radicals, NO_3 radicals, O_3, sunlight, and dilution. The dilution term was estimated in two ways: (1) using CO as a tracer for dilution in the rising planetary boundary layer (PBL) and pollution export from the MCMA (Garcia et al., 2006), and negligible dilution during the night (this method lead to chemical accumulation of oxidation products in the code and is considered a lower limit for dilution); (2) to overcome chemical accumulation in the afternoon and at night, additional dilution was calculated to match predictions of photochemical HCHO with observations (see Sect. 2.4).

HONO photolysis is calculated as the absolute radical flux from HONO photolysis rather than reflecting net-production (i.e., HONO photolysis flux minus the flux from the OH+NO recombination reaction). We feel this is justified because even a negative net radical flux from HONO could still have a positive effect on photochemical radical cycling and ozone formation. This is because the fate of an OH radical is determined primarily by VOC reactions, and only a small portion reacts with NO; a newly formed OH radical thus adds efficiently to the production of RO_2 and HO_2 that recycle OH multiple times before they are removed, and add to the formation of ozone. The net rate of ozone formation due to HONO can hence still be positive, even though the net-production of OH from HONO might be negative. Accounting for HONO on a net-flux basis would not account for this

chemical amplification of radical fluxes from HONO. We accounted for HONO on an absolute flux basis for two reasons: (1) this definition does justice to the true role of HONO to jump start photochemistry during morning hours; and (2) this definition allows us to quantitatively define the concept of "chain length" as the amplification of radical source fluxes (this paper) to radical recycling fluxes (Part 2, Sheehy et al., 2010). It turns out that an OH radical that is produced in the early morning hours is re-cycled about 3–4 times before it is removed by radical sink processes.

In principle, a similar argument could be made for the radical source from the thermal decomposition of Peroxy Acetyl Nitrate (PAN). We have calculated the radical production from PAN, and find that in this urban environment much more PAN is formed than dissociates, to the point that even accounting for chemical amplification of PAN formation is almost exclusively a net radical sink in the near field chemical regime inside the MCMA; hence we have not considered PAN as a radical source. OH radical production rates from the reaction $NO_2^* + H_2O \rightarrow OH + HONO$ was calculated as $P(OH)_{NO_2*} = NO_2 \cdot J(NO_2^*) \cdot q$, where $J(NO_2^*)$ is the non-destructive excitation rate of NO_2, determined from our spectroradiometer data, and $q = 0.001 \cdot k_{H_2O} \cdot [H_2O]/(k_{H_2O} \cdot [H_2O] + k_{O_2} \cdot [O_2] + k_{N_2} \cdot [N_2])$ is the fraction of NO_2^* collisions with water and air molecules that leads to HONO and OH as products; rate constant values are $k_{H_2O} = 1.7 \times 10^{-10}$ molec cm^{-3} s^{-1}, $k_{O_2} = 3.0 \times 10^{-11}$ molec cm^{-3} s^{-1}, $k_{N_2} = 2.7 \times 10^{-11}$ molec cm^{-3} s^{-1} (Li et al., 2008, P. Wine, personal communication, 2007). Notably the OH radical production from further photolysis of any HONO that may form from NO_2^* is accounted among the OH source from HONO.

In order to estimate the nighttime radical production rates from O_3 and NO_3 reactions with alkenes, two scenarios were considered: (1) O_3 constrained (DOAS#1), NO_3 unconstrained; and (2) O_3 and NO_3 constrained by observations. One complication arises from the different sampling altitudes for VOCs, and the mean height of DOAS#2 light beam; vertical gradients in O_3 and NO_3 concentrations are most pronounced at night, and quickly disappear 1–2 h after sunrise. In order to account for vertical gradients in NO_3 radicals (Fig. 2, and Sect. 2.3), as a first-order approximation the observed NO_3 by DOAS#2 was scaled to the altitude of DOAS#1, using a linear scaling factor that was calculated from differences in O_3 as observed between DOAS#1 and DOAS#2 ($[NO_3]_{16\,m} = [NO_3]_{DOAS#2} \cdot [O_3]_{DOAS#1}/[O_3]_{DOAS#2}$). The O_3 data measured by both LP-DOAS are shown in Fig. 3. The scaled NO_3 concentrations were on average about a factor of 3 lower (nighttime 8 h average concentration of 1.5 pptv), and are regarded as an upper limit of the true concentration at the height of DOAS#1 since nonlinear feedbacks are not accounted for. We further base our discussion of NO_3 radicals on the (unverified) assumption that similar VOC concentrations are present in NO_3-rich and
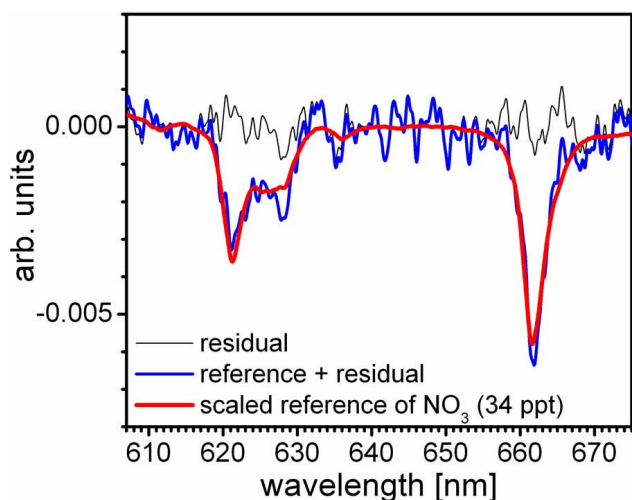
Fig. 2. Spectral proof for the detection of NO_3 radicals in Mexico City (29 April 2003, 01:17 a.m. CST). The atmospheric spectrum (blue line) has been corrected for NO_2, and water absorptions, and shown with an accordingly scaled NO_3-reference spectrum (red line) from our previous work.

NO_3-depleted air masses. As reactive unsaturated VOCs are expected to be depleted in O_3- and NO_3-rich air, this assumption is compatible with an upper limit estimate of the role of NO_3 radicals as a source for RO_x radicals at the roof-top level. These uncertainties were minimized by constraining the box-model with data collected at roof-top level (also DOAS#1 height). Finally, the sensitivity of the model towards statistical artifacts was tested by constraining with (1) average, and (2) median time-profiles of the above measurements; the results agreed within 10% at daytime, whereas larger differences were observed at night (see Sect. 3.3). Unless otherwise noted the results are reported from the model constrained by the median time series data.

2.3 Characterization of horizontal and vertical gradients

A possible complication in constraining the MCM model might arise from the fact that measurements used to constrain the model are conducted over extended spatial scales (LP-DOAS, FTIR) and in the form of highly localized "point" measurements (e.g., PTR-MS). The direct comparison of radical fluxes inferred from these measurements is based on the assumption that the air mass is well mixed. This assumption is tested below, and appears to be justified for the following reasons. Spatial gradients are expected to be strongest for primary pollutants (e.g., CO) and somewhat less pronounced for secondary pollutants (e.g., O_3). Sampled concentrations of CO and O_3 at comparable heights by point and line-averaging techniques at the CENICA supersite show excellent agreement (Dunlea et al., 2006). Further, concentrations of several species that were probed by
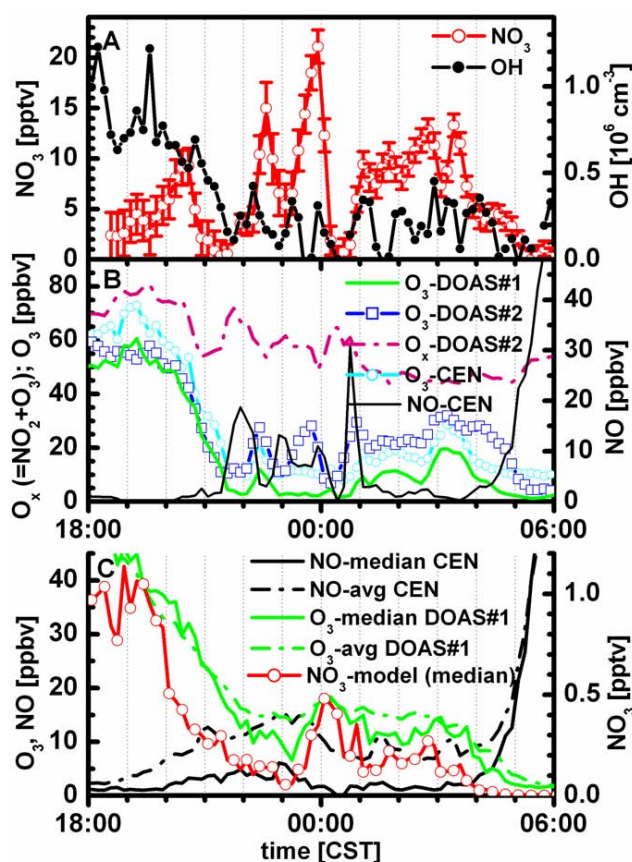

Fig. 3. Nighttime concentration-time profiles of NO_3 radicals and OH radicals during the night from 25 to 26 April 2003 **(A)**, O_3 (from two LP-DOAS and a point sensor), O_x (sum of O_3 and NO_2) and NO **(B)**. Panel C compares average and median nighttime O_3 and NO concentrations, and shows NO_3 radical predictions from the median model. The nighttime OH concentration tends to follow the time trace of O_3 better than that of NO_3 radicals.

both open-path DOAS instruments facing in different directions, spanning different spatial scales and sampling at different mean heights show excellent agreement during the day (within measurement precision). For example, HONO was measured by two LP-DOAS instruments at 16 m and 70 m above ground, and vertical gradients are observed at nighttime and in the early morning. However, the data from both instruments have converged to within measurement precision already 1.5 h after sunrise (06:00 a.m. CST), as illustrated for HONO in Fig. 4. During the daytime, which is the primary focus of this study, the air mass is thus considered to be well mixed.

At night, mixing is driven by the heat-island effect (Jauregui, 1993; Oke et al., 1999) and large-scale eddy turbulence from mechanical sheering of winds aloft which can lead to horizontal and vertical gradients in trace-gas concentrations. Comparison of the measurements from the two LP-DOAS instruments with point sampling techniques set the limits on
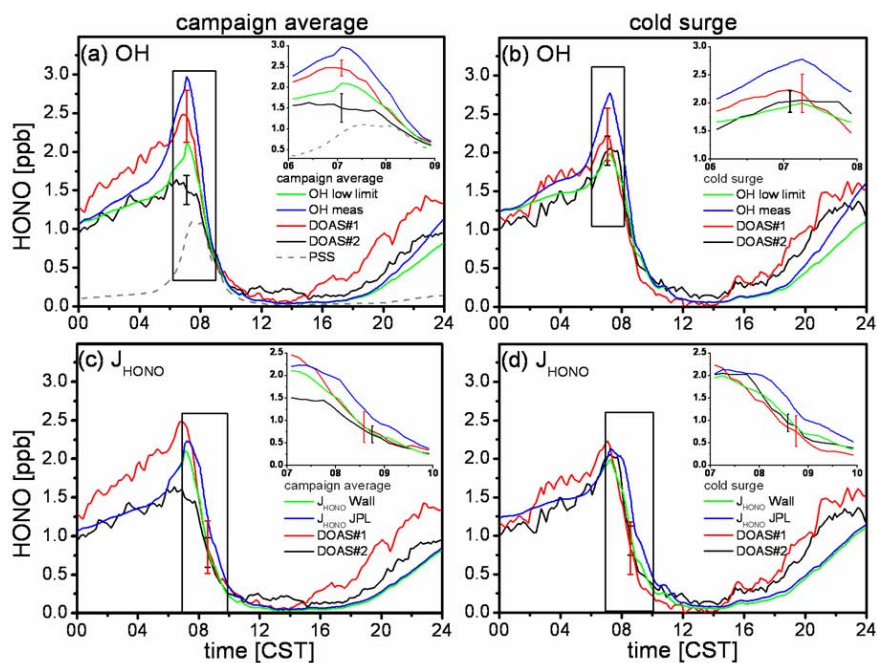
Fig. 4. Measured (red, black) and calculated (green, blue) HONO concentrations. Shown are campaign-averaged data **(a, c)** and data averaged over cold-surge events **(b, d)**. The top two graphs show that varying OH within uncertainty (lower limit) improves the model measurement agreement in the early morning. The bottom two graphs show that model predicted HONO is systematically higher than the observations during mid- morning; an additional HONO sink is needed. Use of a higher value of J_{HONO} according to Wall et al. (2006) improves the agreement between measured and modeled HONO concentrations significantly.

this inhomogeneity (see Figs. 3 and 4). Significant vertical gradients are observed for HONO and ozone. In an attempt to minimize the effect of vertical gradients on the prediction of secondary sources we chose to interpolate vertical gradients in oxidants to assure that constraints to the MCM model are at a comparable height (OH, O_3, NO_3). For the most precise measurements of low O_3 concentrations, we use direct measurements from DOAS#1 (for a discussion of possible interference issues with indirect techniques see Dunlea et al., 2006). NO_3 radical concentrations at higher altitudes are adjusted here to roof level (Sect. 2.2). Figure 3a illustrates the significant variability in NO_3 concentrations in our line-averaged detection of several kilometers spatial scale. Periods of steeply rising NO concentrations are followed by periods when essentially no NO_3 is observed. Also shown are the O_3 concentrations measured by both LP-DOAS and a point-sensor, the sum of NO_2 and O_3 (O_x, from DOAS#2), and NO during that night (Fig. 3b). The good agreement in the relative variation between the point-sensor and DOAS#1, which are located at comparable altitudes, illustrates that at night the air mass is relatively homogeneous over horizontal spatial scales on the order of few 430 m. The 5–10 ppbv offset in the point sensor is probably not real, as is discussed in Dunlea et al. (2006).

Implications of nighttime inhomogeneities for the MCM model

The simultaneous presence of O_3 and NO in the same air mass has implications for RO_2-to-OH conversion efficiencies, predicted NO_3-radical concentrations, and, to a lesser extent, OH production rates. Figure 3c shows the comparison of the median and average concentration time profiles of O_3 (DOAS#1) and NO (point sensor). During the day there is virtually no difference between the average and median profiles, reflecting efficient mixing. At night, median concentrations are systematically lower for both O_3 and NO. The difference is larger for NO (a factor to 5–8) than for O_3 (10–80%), and reflected in the predicted NO_3-radical concentration at the roof-top-level (about five times higher; median NO_3 concentrations are shown in Fig. 3c). The average lifetime of O_3 with respect to NO reactions at night is considerably longer in the median model (about 15 min; compared to about 2.5 min in the average model), i.e., long enough that the presence of both O_3 and NO in the same airmass is feasible based on their respective reactivity. Based on these results we prefer the median model for estimates of ΣOH_{new}, which is reduced by one-third at night compared to the average model.

2.4 Source apportionment of photochemical HCHO calculations

We attempted to identify the relevance of different classes of VOC to the photochemical production of HCHO. We used the above-mentioned box model, without the HCHO constraint, to predict the rate of HCHO production from hydrocarbon oxidation chemistry during mid-morning conditions. The model was initiated using a constrained VOC split as given in the Supplementary Information of Sheehy et al. (2010), and oxidant and light conditions were kept constant: [OH]=0.18 pptv, [O_3]=55 ppbv and J_{NO_2}=5×10^{-3} s^{-1}. The fate of peroxy radicals is about 90% determined by reactions with NO in our model, which is consistent with the modeling of field data at peak photochemical productivity during mid-morning hours (see Fig. 6 in Sheehy et al., 2010). In a first set of model runs, the contributions from individual VOC classes as HCHO precursors were calculated by tracking the rate of HCHO production and varying the VOC split; only a single VOC class was set to non-zero, while the other VOC concentrations were set to zero. Second, to determine the relative contribution of individual oxidants, the rate of HCHO production was calculated with only that oxidant i.e., OH, O_3, NO_3; the other oxidant concentrations were set to zero; identical sets of VOC and kinetic parameters were used. Third, to calculate the percentage of HCHO production as a first or higher generation VOC oxidation product, the yield of photochemical HCHO was compared after 10 min and several hours of oxidation (see Volkamer et al. (2001) for details on the argument). Only a small increase in the rate of HCHO production was observed over extended oxidation times, indicating that some HCHO is indeed produced as a higher generation oxidation product from OVOC oxidation, but this fraction is rather small (16%). Most HCHO predicted from the MCM is thus formed as a first generation oxidation product. For most VOCs that are constrained in the model from the MCMA-2003 dataset, the formation of HCHO has been studied in the laboratory. The chemical pathways represented in the MCM are thus largely based on experimental constraints, and only a minor portion of predicted HCHO is expected to be formed from pathways that might be subjected to the more uncertain structure-reactivity relationships that (to a larger extent) underlie the MCM representation of OVOC oxidation.

Sensitivity studies using the flexible top MCM box model revealed that predicted HCHO accumulated to unrealistic concentrations later in the day. This prompted us to investigate whether the cause of this overestimation in the afternoon was due to uncertain chemical pathways that form HCHO in the model, or to an underestimate of pollution export (dilution). Photochemical sources from HCHO turned out to be well constrained (see above, and also Sect. 3.5). It was concluded to adjust the dilution sink of HCHO in the model to bring predicted HCHO in the later day into agreement with the photo- chemically formed portion of observed

HCHO (Sect. 3.5). We used a modified Eq. (1) in Garcia et al. (2006) to calculate the photochemically formed portion of ambient HCHO: [HCHO]$_{phot}$=[HCHO]$_{meas}$ − 0.0015· [CO], where the latter term represents a scaled tracer for HCHO emissions according to results from Garcia et al. (2006). The additional dilution reduced the afternoon HCHO by a factor of about 2.

2.5 Source apportionment of HONO calculations

The sources of HONO investigated include photo-stationary-state HONO (PSS-HONO; under equilibrium conditions PSS-HONO=k·OH·NO/J_{HONO}), dark sources from the OH+NO recombination reaction, heterogeneous formation on urban surfaces, or aerosols, and photochemical sources. The MCM model is constrained by measurements of OH, NO, J_{HONO}, dilution, and we used the model to calculate PSS-HONO. Nighttime OH only explained a small increase in HONO concentrations over the course of a night, and an additional HONO source was parameterized as a $NO_2 \rightarrow$HONO conversion rate to match the HONO production between 08:00 p.m. to 04:00 a.m.; this "dark-HONO" source was then applied throughout the day.

We employed the box model in the following three scenarios: inputs are constrained based on (1) campaign average concentration time-profiles, and (2) median concentration time-profiles. In an additional model scenario (3), only data from "cold-surge" days were averaged (de Foy et al., 2005), which are characterized by the highest relative humidity and the lowest PBL height. The highest daytime HONO concentrations are expected during such "cold-surge" events, as HONO concentrations have been shown to correlate with relative humidity (Stutz et al., 2004). For each of the three model scenarios, the sensitivity of the model output was tested by varying the OH concentration within measurement uncertainty (offset of 0.01 pptv was subtracted), varying the dilution case, and varying J_{HONO} within twice the experimental uncertainty (multiplication of J-value based on (Stutz et al., 2000) by 1.43 reproduces our observations, and is in general agreement with recent direct measurements of J_{HONO} by Wall et al. (2006) that indicate scaling by a factor of 1.28). Any photochemical sources are evaluated as the difference to model predicted and "observed" daytime HONO. The model generally predicted HONO concentrations that were consistent with measured concentrations in the morning.

2.6 Radical production from oxygenated VOC (OVOC) photolysis

Selected OVOC such as HCHO, CHOCHO and CH_3CHO, and their respective photolysis frequencies were measured during MCMA-2003. Other OVOC, a complex mixture of several hundred VOC reaction products, were estimated using the MCM model. The radical initiated OVOC loss is

neutral in terms of radical production, since in principle the radical that is consumed by initiating the oxidation leads to the formation of another radical (i.e., a RO_2 radical). On the other hand, OVOC photolysis converts a closed shell OVOC molecule into two radicals and is an efficient radical source. The model was constrained using measurements of $J(NO_2)$ and the other photolysis parameters were parameterized relative to $J(NO_2)$ in the model.

In Table 1 the production of OH, HO_2 and RO_2 from OVOC photolysis is tracked using the constrained MCM model (for details see Part 2), and summed for a number of compound classes, i.e., aldehydes, multifunctional carbonyls, epoxides, ketones, and other miscellaneous OVOC. Aldehydes (RCHO in Table 1) are counted as the reaction of (multifunctional) carbonyls with only one end standing carbonyl group. The photolysis happens at the end-standing carbonyl group (associated with J-values 11, 15, and 17 in the MCM code). This group does not include HCHO, which is constrained in the model, and represented separately in Table 1 (see above). Carbonyls are counted as the flux from more complex molecules, which typically have 2 or 3 carbonyl groups, and photolysis is associated with J-values 4, 34, and 35 in MCM. This group includes dicarbonyls other than glyoxal, which is constrained in the MCM and represented separately in Table 1. Epoxides (EPOX) are characterized as compounds with more than one functional group; however, photolysis occurs at the epoxy functional group (note that both dicarbonyls and epoxides are associated with J-value 4 in the MCM, and our lumping actually considers the structure of the molecule as a means to differentiate the lumping). Ketones (KETO) are grouped as compounds that generally have more than one functional group; however, the photolysis occurs at the ketone group. This group is associated with J-value 22 in the MCM code. Other miscellaneous OVOC (MISC) are compounds that photolyze with J-values 18 and 19. Hydroperoxides (ROOH) are lumped as the flux from reactions that photolyze with a J-value 41.

The radical fluxes from OVOC are taken from the MCM model that applied the increased dilution rate scaled from photochemical HCHO (Sect. 2.4) to all other predicted OVOCs.

3 Results and discussion

3.1 OH-equivalent RO_x radical production rates

The calculated production for new RO_x from the HO_x-constrained box model is shown in Fig. 1. The total radical production rates presented in the bottom panel are shown as OH-equivalents, termed ΣOH_{new}, and account for the conversion factors in the radical propagation steps, i.e., $RO_2 \rightarrow OH$ and $HO_2 \rightarrow OH$, as described in more detail in Part 2 (Sheehy et al., 2010). Figure 1 is accompanied by Table 1, which shows the percent contribution to ΣOH_{new} from

various sources at selected times throughout the day, as well as day and nighttime averages. Pathways with an insignificant contribution are not shown.

The daytime ΣOH_{new} around noon is about 25 times larger than at night. A distinct diurnal pattern is observed. Radical production rates are high already shortly after sunrise (2 ppb h^{-1}, or 1.1×10^7 molec cm^{-3} s^{-1} at 07:00 a.m.), predominantly due to the production of OH radicals. The production rates continue to rise and reach a plateau in the mid-morning (13 ppb h^{-1}, or 6.9×10^7 molec cm^{-3} s^{-1} at 10:00 a.m.). Sustained radical production persists at high level until about 12:30 p.m. and begins to decrease afterwards. A continuous decrease in radical production is observed during afternoon hours until about 06:00 p.m. (1.0 ppb h^{-1}, or 5.4×10^6 molec cm^{-3} s^{-1} at 06:00 p.m.). Radical production rates remain flat until the early morning hours. The decrease in OH, HO_2, and RO_2 radical production rates during afternoon hours coincides with decreasing O_3 concentrations due to pollution export from the MCMA, and reflects the strong coupling between the abundance of secondary pollutants and photochemical activity.

The 12-h daytime average ΣOH_{new} (6.5 ppb h^{-1}, or 3.5×10^7 molec cm^{-3} s^{-1}) is equally attributable to OH and HO_2 sources (both about 40%), while RO_2 sources contribute about 20%. The photolysis of secondary OVOC other than HCHO accounts for about 33% of ΣOH_{new}. ΣOH_{new} from other OVOC is 60% due to new HO_2 formation, and 40% due to new RO_2 formation. O_3 and HCHO are the most important single molecule radical sources in the MCMA, and are equally important (20% each). The O_3/alkene source adds nearly 15%, with new OH- and RO_2 production contributing about equal amounts. HONO contributes about 12% over this average period, and is more important in the morning. Our model estimates an average daytime NO_3 radical concentration of about 0.6 pptv and about 1 pptv around noon. Daytime NO_3 radical reactions make a very small contribution to daytime ΣOH_{new}, reflecting high NO concentrations, and the fact that radical production rates from other sources are comparably large.

During the night, the ΣOH_{new} is determined from the reaction of alkenes with O_3 and NO_3. The 8-h nighttime average (08:00 p.m.–04:00 a.m.) ΣOH_{new} (0.48 ppb h^{-1}, or 2.6×10^6 molec cm^{-3} s^{-1}) is dominated by O_3/alkene reactions. The OH and RO_2 sources contribute roughly similar amounts, and in sum account for about 80% ΣOH_{new}; new HO_2 accounts for a minor radical source at night. The only direct nighttime source of OH and HO_2 radicals is the reaction between O_3 and alkenes. On the other hand, for practical purposes the reactions of alkenes with NO_3 exclusively generate new RO_2 radicals. The model suggests that such NO_3/alkene reactions account for some 8–24% of nighttime ΣOH_{new}; the remaining new radical production is from O_3/alkenes. If we force the scaled upper limit 8-h average NO_3 radical concentration of 1.5 pptv at night (about six times the predicted values), then the reaction between NO_3

and alkenes could account on average for about half of night-time ΣOH_{new}. However, such scaled NO_3 concentrations do not account for the rapid NO_3 sink reaction with NO (see Sect. 3.3, and Fig. 3), and the actual ΣOH_{new} from NO_3 at roof-top-level is likely much lower. In the near field chemical regime at roof-top-level, the NO_3/alkene source is a minor pathway for ΣOH_{new} at night.

3.2 Production of OH, HO$_2$, and RO$_2$ radicals

3.2.1 Sources for OH radicals

The production of OH radicals from sources is high ($4\,ppb\,h^{-1}$, or $2.1\times10^7\,molec\,cm^{-3}\,s^{-1}$) about two hours after sunrise, and near constant throughout the morning. It starts to decrease after noontime (12:00 p.m. CST), and is at least an order of magnitude lower at night. The predominant daytime OH radical sources are: (1) the photolysis of HONO, (2) the photolysis of O_3, and (3) the O_3/alkene reactions. In the early morning hours, the photolysis of HONO dominates the formation of OH radicals. As photochemical O_3 accumulates, the photolysis of O_3 becomes a dominant source of OH in the late morning and throughout most of the day, accounting for about 80% at peak ozone levels. It is noteworthy that small but "non-zero" O_3 concentrations in the presence of high alkene concentrations during early hours, and unmeasured products from nighttime processing of VOCs present a significant source for OH radicals other than HONO in the early morning. Few ppb of O_3 coexist with several 10 ppb of NO shortly after sunrise, and contribute about 20% to OH production, illustrating how small changes in ozone may have a significant effect on OH radical production rates at this time of day. Difficulties with the exact quantification of low O_3 levels exist for indirect techniques, which are widely used in current air quality monitoring networks (see discussion in Dunlea et al., 2006). An additional uncertainty exists in the speciation of alkenes, which can be affected during sample storage (Atkinson et al., 1984; Jenkin et al., 2005). OH production from O_3/alkenes is the only significant gas-phase non-photolytic source of OH during the day and at night.

3.2.2 Sources for HO$_2$ radicals

The production of HO$_2$ radicals is smaller than that of OH shortly after sunrise, and continuously increases to reach values around $5.8\,ppb\,h^{-1}$ (or $3.1\times10^7\,molec\,cm^{-3}\,s^{-1}$) around noontime. As in the case of OH, it starts to decrease after noon. New HO$_2$ is only a significant radical source during the day; the new HO$_2$ production is at least two orders of magnitude lower at night. The predominant daytime sources for HO$_2$ are (1) the photolysis of HCHO, and (2) the photolysis of other secondary OVOCs. HCHO photolysis accounts for more than half, the sum of other OVOCs for about 45% of the midday HO$_2$ production. The photolysis of CH_3CHO

and O_3/alkene reactions contribute less than 2% new HO$_2$ radicals throughout the day. During the night the only significant HO$_2$ radical source is from O_3/alkene reactions.

3.2.3 Sources for RO$_2$ radicals

The diurnal profile of RO$_2$ radical production is qualitatively similar to that of HO$_2$ radicals, though peak values around noontime are smaller ($3.8\,ppb\,h^{-1}$, or $2.0\times10^7\,molec\,cm^{-3}\,s^{-1}$ at 10:00 a.m.). Also, the new RO$_2$ production rate is about an order of magnitude lower at night, compared to peak daytime production. The predominant daytime sources for RO$_2$ are the photolysis of secondary OVOCs, accounting for nearly 78% of new RO$_2$ radical production at midday, and about 66% on a 12-h daytime average basis. Some minor additional RO$_2$ is produced from O_3/alkene reactions and reactions of NO_3 with alkenes, phenol- and furanone-type products of the OH-radical initiated oxidation of aromatic hydrocarbons. While these reactions only account for a minor source of RO$_2$ radicals, they provide an interesting link between the RO$_x$ and NO$_x$ cycles (see Sect. 3.3).

3.3 Direct observations of NO$_3$ radicals

NO$_3$ radicals were detected during all nights that measurements were attempted. The spectral proof of the successful detection is presented in Fig. 2. The highest optical density of NO$_3$ radical absorption was 9.6×10^{-3}, corresponding to a concentration of $(9.6\pm1.1)\times10^8\,mole\,cm^{-3}$ or (50 ± 6) pptv. The nighttime concentration-time profile varied between individual nights. Typically, detectable concentrations were observed during events that lasted 1–3 h. The NO$_3$ concentrations typically peaked around midnight (±2 h), sometimes also later in the evening, and varied between 10 and 50 pptv. The nighttime average NO$_3$ mixing ratio for all nights (19:00–04:00) is about 7 pptv (at DOAS#2 heights). No NO$_3$ was detected during the afternoon hours and the early evening prior to sunset, and concentrations were below the detection limit during early morning hours. To our knowledge this is the first direct detection of NO$_3$ radicals in the urban core of a megacity.

Interestingly, our direct NO$_3$ radical observations at a mean height of 70 m above ground pose an apparent conundrum to explain inferences of negligible NO$_3$ chemistry at the CENICA roof-top level: An isomer-analysis of nitro-PAH samples revealed a very minor contribution of NO$_3$ radicals to PAH processing (Arey et al., 2004). It is noteworthy that negligible NO$_3$ radical concentrations are predicted at rooflevel by MCM, and low NO$_3$ at roof level is also expected based on our scaling procedure to account for vertical gradients (Sect. 2.2). However, nitro-PAHs are sufficiently long lived that they should be observable at roof level if indeed formed, and thus the absence of nitro-PAHs at roof level contains relevant (and potentially important)

information about the processing of primary pollutants at night. Freshly emitted PAHs are collocated in plumes that contain elevated NO, which rapidly destroys NO_3 radicals: $NO_3+NO \rightarrow NO_2$. This is corroborated in Fig. 3, where elevated NO_3 concentrations tend to correlate with elevated O_3, while air masses with higher NO_2 (lower O_3) tend to contain virtually no NO_3. We conclude that even though NO_3 radical concentrations of 50 ppt are observed, this should not be taken as evidence that primary pollutants, like PAHs, are easily processed by NO_3 radicals at night.

3.3.1 Does NO_3 contribute to nighttime OH?

Nighttime OH radical concentrations are currently not well understood and subject to ongoing debate. As shown in Fig. 3, the nighttime OH concentration correlates better with O_3 than with NO_3 in the early evening. This is true also, though to a lesser extent, in the later night hours. However, a conclusion on whether O_3 or NO_3 control the nighttime OH concentration is complicated by the fact that both gases tend to be correlated. From the discussion presented in Sect. 3.1, it is likely that NO_3 radicals make a minor and possibly significant contribution, to nighttime OH radical concentrations already in the near field chemical regime. The occurrence of NO_3 concentrations in episodes, and the lack of co-located open-path NO data observed in the same air mass as NO_3, makes it difficult to compare with a median model. Like NO, NO_3 radicals facilitate the cycling of RO_2 and HO_2 into OH. It is noteworthy that the propagation efficiency of RO_2 into OH radicals is controlled by NO in our model; NO_3 reactions are negligible in all cases studied. Different conditions are expected in the intermediate and far-field photochemical regime, i.e., NO_3 enriched air masses at altitudes of several hundred meters above ground, and in the O_3-rich city plume downwind of the MCMA. In similar air masses, NO_3 concentrations of several hundred pptv have been observed (von Friedeburg et al., 2002; Brown et al., 2006). Under these conditions NO is very low; the efficiency of RO_2 radicals to propagate into OH radicals ($RO_2+NO_3 \rightarrow RO+$products; $RO+O_2 \rightarrow HO_2+$products; $HO_2+NO_3 \rightarrow OH+$products) conversions is controlled by NO_3 reactions, which proceed more than an order of magnitude slower than the analogous reaction involving NO; NO_3 competes with peroxy-radical self reactions which can terminate the radical chain. The efficiency for $RO_2 \rightarrow OH$ conversion is thus lower than in a high NO scenario such as ours. A possible exception could arise from recent findings that peroxy-radical self reactions propagate the radical chain (Hasson et al., 2004; M. E. Jenkin, personal communication, 2006). If these reactions were confirmed as a more general pathway, NO_3 reactions would gain importance as a source for nighttime OH-radical in the intermediate and far-field chemical regime downwind of large urban centers. Our model indicates that NO_3 does not contribute much to nighttime OH production at roof level during MCMA-2003.

3.3.2 Processing of furanones by daytime NO_3

We did not find evidence of NO_3 radicals accumulating to measurable concentrations during the day in Mexico City. This is in contrast to Houston (Geyer et al., 2003), and New England (Brown et al., 2005), where daytime NO_3 concentrations have been observed, and form a non-negligible process for the oxidation of highly reactive VOC. This difference is the result of lower O_3 during afternoons, and likely also significant NO_3 sink reactions in Mexico City. In contrast to Houston, biogenic VOC concentrations are much lower in Mexico City (quantified as <5% of OH-reactivity during MCMA-2003 in Volkamer et al., 2006).

However, the daytime NO_3 radical concentration is on the order of 0.5–1 ppt in our model. NO_3 reactions with anthropogenic alkenes, phenol-type and furanone-type products from aromatic hydrocarbon oxidation contribute about 26%, 36%, and 15% of the daytime RO_2 sources from NO_3-reactions, respectively. These reactions account in sum for about 7% of the daytime NO_3-sink reactions, and thus can compete with rapid NO_3 photolysis and NO reactions for NO_3 radicals. The NO_3 production rate at 100 ppb O_3 and 10 ppb NO_2 is about 1.3×10^7 molec cm^{-3}, and the overall flux through NO_3+VOC reactions is ca. 10^6 molec cm^{-3} s^{-1}. Daytime NO_3-reactions with furanones account for some 5–15% of the furanone lifetime in our model. The relevance of daytime NO_3-reactions, previously noted only for phenols (Kurtenbach et al., 2002), is highlighted here also for furanone-type compounds.

3.3.3 N_2O_5 uptake to aerosol: a likely source for nitryl chloride in the MCMA

O_x (sum of NO_2 and O_3) is found to decrease at a rate of 2.1 ppb h^{-1} at night, see Fig. 3. This loss of O_x is attributed to the combination of various factors: (1) O_x to NO_y conversion processes, such as N_2O_5 hydrolysis on aerosols and ground surfaces, (2) dry deposition of O_x or NO_y, and possibly also (3) pollution export from the MCMA.

The heterogeneous uptake of N_2O_5 can trigger reactions with Cl^- that can lead to the formation of nitryl chloride ($ClNO_2$) (Finlaysson Pitts et al., 1989), and molecular chlorine (Cl_2) (Roberts et al., 2008). This reaction is accelerated under acidic conditions, which are typical for particles in Mexico City (e.g., pH$\sim$4, Volkamer et al., 2007). We note that aerosols were mostly aqueous during MCMA-2003, and contained non-negligible amounts of chloride (San Martini et al., 2006). Assuming an N_2O_5 concentration of 0.2 ppb, an N_2O_5 uptake coefficient $\gamma=0.01$ (compare e.g., Brown et al., 2006), and a typical condensable sink aerosol surface area $S=400$ mm^2 m^{-3} (compare Fig. 1 in Volkamer et al., 2007, at night), the heterogeneous N_2O_5 uptake to aerosols can account for about 3 ppb N_2O_5 loss over 12 h. Cl^- concentrations often are above 0.1 M in Mexico City aerosols (San Martini et al., 2006), and under those conditions N_2O_5

is efficiently converted into $ClNO_2$ (Behnke et al., 1997; Roberts et al., 2008). Based on this rough estimate we attribute a significant, though likely not major portion of the observed O_x losses (on the order of 10%, or 2–3 ppb) to the formation of $ClNO_2$.

3.4 Source and sink considerations of HONO

HONO is heterogeneously formed at night, and is an important radical source in the early morning (Platt et al., 1980), yet our understanding of the HONO sources remains incomplete. The constrained MCM model is found to predict HONO surprisingly well. The measured HONO profiles from DOAS#1 and DOAS#2 are compared with HONO predictions in Fig. 4. Regardless of the meteorological conditions, PSS-HONO accounts for at least half of the HONO concentrations at 07:00 a.m., and virtually all HONO at 09:00 a.m. Figure 4 demonstrates that a small OH concentration in the presence of high morning NO concentrations account for ppbv-levels of HONO at 08:00 a.m. Few previous studies had simultaneous and collocated OH, NO, HONO and J_{HONO} measurements available; the interpretation of most HONO as being a radical reservoir is fully consistent with the error bars presented in Fig. 3 of Martinez et al. (2003). Additional HONO formation from dark sources, like the heterogeneous NO_2 conversion on urban surfaces (see, e.g., Arens et al., 2001; Ramazan et al., 2006 and references therein) do appear to contribute significant amounts of HONO only before 08:00 a.m. Thereafter PSS-HONO (and a minor contribution from dark HONO sources) account for essentially all of the observed HONO. Around solar noon the PSS and dark sources can account for some (35±15) pptv; these model results are robust for different meteorological conditions and independent of relative humidity. This is of the same order of magnitude as the upper limit HONO concentration that can be inferred from the DOAS#2 detection limit. Statistical averaging of DOAS#2 data yields (58±76) pptv and (21±76) pptv HONO on a campaign average and median basis; error bars correspond to one-sigma standard-deviation among individual days around solar noon. An independent quantification of daytime HONO concentrations in Mexico City remains desirable. However, it is noteworthy that photo-induced processes (included in "dark+other" HONO sources in Table 1) appear to contribute – if any – only very minor amounts to ambient HONO concentrations in Mexico City. For example, a photochemical HONO source of 5×10^{10} molec cm^{-2} s^{-1} from the ground (Stemmler et al., 2006), diluted in a PBL of 3 km height (typical for Mexico City), corresponds to a HONO mixing ratio of only 4.3 pptv around noon.

The characterization of daytime HONO sources in the urban atmosphere – if attempted in the future – suffers from the need to subtract a large steady-state HONO concentration. This steady-state HONO can only be quantified at the precision with which the reaction rate constant of OH with

NO is known, i.e., 20% (Sander et al., 2006); in our estimate the largest uncertainty is the absolute uncertainty in OH measurements. For example, in order to quantify a photo-induced HONO concentration of 25 pptv on top of a 25 pptv PSS-HONO background with 25% uncertainty, the absolute precision of OH measurements needs to be 15% or better; such measurements are currently very difficult to achieve. High precision measurements of HONO (Kleffmann et al., 2006), NO, and J_{HONO} are necessary – though unlikely to be limiting – for efforts to quantify excess HONO over PSS-HONO in the urban atmosphere.

Faster than expected HONO photolysis?

We observe a significant delay in the decrease of HONO in the model if J_{HONO} is based on the value listed in Sander et al. (2006). Notably, by 09:00 a.m. the contribution of dark HONO sources makes a very small contribution (<10%, see Table 1), and HONO concentrations between two DOAS instruments agree well. This indicates that uncertain scaling of dark HONO sources and vertical gradients do not appear to limit our measurement-model comparison at 09:00 a.m. The difference between measured and modeled HONO concentrations persists for several hours in the morning (see inset of Fig. 4) until HONO concentrations fall to values close to the detection limit. Model predicted HONO exceeds the observations by about 70% at 09:00 a.m., when uncertainty in PSS-HONO production rate is on the order of ~40% and uncertainty in the HONO measurements by DOAS#2 is ~35%. Model predicted HONO and observed HONO are only marginally in agreement. The over-prediction of HONO in the model indicates that a HONO sink is missing in the model. By scaling our J_{HONO} by 1.43 we observe good agreement between the model and measurements throughout the day (see Fig. 4, lower panels); scaling by 1.22 brings the predicted HONO into marginal agreement with DOAS#2 error bars.

Recent direct measurements of J_{HONO} reported values that were about 1.28 times higher than expected (Wall et al., 2006). Uncertainties in the absolute values of the HONO absorption cross-section arise from necessary "offset" corrections due to lamp drifts in the currently recommended HONO cross section (Stutz et al., 2000; Sander et al., 2006), which can account for about 1.13 to 1.2 times faster HONO photolysis (Stutz et al., 2000; Bongartz et al., 1991). In principle OH overtone pumping by visible and infrared photons can also lead to additional HONO photolysis from the electronic ground state (Donaldson et al., 1997). This process is more important at higher altitudes (Witonsky et al., 2001), but could make a minor contribution at the altitudes of Mexico City. We find independent evidence for faster-than-expected HONO photolysis that – within error bars – can probably be rationalized from uncertainties in the UV spectral range. A reduction in the offset uncertainty in the currently recommended UV spectrum remains desirable.

3.5 Source apportionment of HCHO

The observed formaldehyde concentrations in the MCMA
are a result of emissions, photochemistry, and an unknown
background source, which is generally small (1–2 ppb) and
appears to be related to a VOC chemical source (Garcia et
al., 2006). The atmospheric lifetime of HCHO in the MCMA
is on the order of 1–2 h; sustained and elevated concentra-
tions of HCHO in the MCMA are thus an indicator that
HCHO is constantly formed from these sources throughout
the day. Garcia et al. (2006) demonstrated that on a 24-h av-
erage basis, up to 70% of observed HCHO in the MCMA is
photochemically produced. Measured ambient HCHO, and
the portion from photochemical and background sources are
compared with the MCM predictions in Fig. 5. The lower
limit nighttime OH concentration leads to accumulation of
several ppb of HCHO (not shown), consistent with the in-
terpretation of "background HCHO" from a chemical source
(Garcia et al., 2006). Directly emitted HCHO is more rele-
vant during morning hours, and photochemical sources are
the most significant about 2 h after sunrise. Direct HCHO
emissions are important to help jump start photochemistry
(Lei et al., 2009), but become less important to sustain ozone
and SOA formation in the mid-morning and later when pho-
tochemical sources of HCHO dominate.

MCM was used to characterize photochemical HCHO pro-
duction in terms of: (1) the relative contribution of HCHO
sources by VOC class (i.e., alkanes, alkenes, aromatics,
OVOCs); (2) the relative contribution of oxidants, i.e., OH,
O_3, and NO_3; and (3) the portion of HCHO formed as a
first vs. second (and higher) generation oxidation product.
The results of the HCHO source apportionment modeling
are shown in Fig. 6. On a daily average basis, we find that
an overwhelming majority of the photochemical HCHO pro-
duction proceeds from reactions that yield HCHO as a first
generation oxidation product. The oxidation of alkenes is
the major VOC precursor, and OH is the predominant oxi-
dant that leads to the formation of photochemical HCHO in
the MCMA. The O_3/alkene source, while significant, only
accounts for some 17% of the photochemical HCHO pro-
duction. The aromatic species make a smaller contribution,
and are largely responsible for secondary HCHO production.
NO_3 radical initiated oxidation of VOCs and photolysis re-
actions are insignificant compared to other sources of HCHO
in the MCMA.

3.6 Comparison of Mexico City with other case studies

Detailed studies for radical production are available for com-
parison from Los Angeles (Griffin et al., 2004), Nashville
(Martinez et al., 2003), Pabsthum downwind of Berlin (Al-
icke et al., 2003), New York City (NYC; Ren et al., 2003),
Milan (Alicke et al., 2002), Birmingham (Emmerson et al.,
2005), Chelmsford downwind of London (Emmerson et al.,
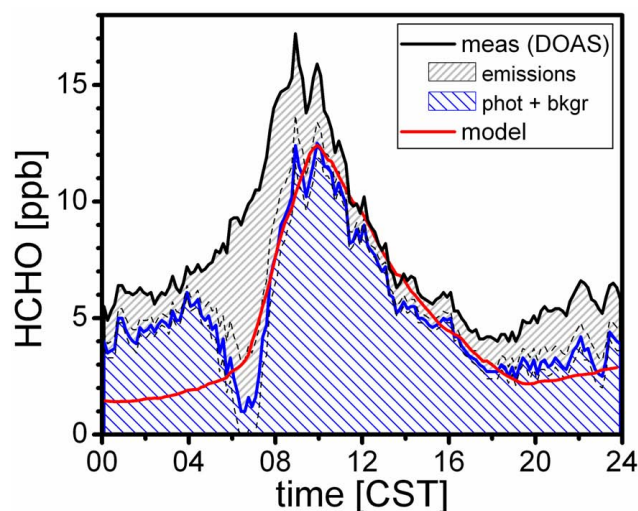2007), rural environments (Zhou et al., 2002; Kleffmann et

Fig. 5. HCHO observations (black line) are compared to the portion
of HCHO produced from photochemical sources and background
sources (blue line, shaded blue area), and from emissions (shaded
gray area); the dotted lines represent the upper and lower limits of
subtracting out emissions sources according to the procedure de-
scribed by Garcia et al. (2006). Modeled HCHO concentrations
(red line) are shown in which dilution was adjusted to match the
blue line (after 10:00 a.m., see Sect. 2.2).

al., 2005; Acker et al., 2006) and the free troposphere (Singh
et al., 1995; Arnold et al., 2004).

3.6.1 Timing of radical production

It is generally expected that the radical production rate during
summer follows the abundance of sunlight and peaks around
the time of lowest solar zenith angle (solar noon). Such cor-
relations are indeed observed in NYC, Nashville, rural en-
vironments and also during cleaner days in Pabsthum and
Milan, while peak radical production is shifted towards early
afternoon hours in Los Angeles. There is only limited in-
formation given about the timing of radical production in
Birmingham and Chelmsford, though the choice of averag-
ing times in the presentation of the results from those stud-
ies (11:00 a.m.–03:00 p.m., centered around solar noon), and
the relative importance of photolytic sources may be indica-
tive of such correlation during summertime. Alternatively,
a radical pulse from HONO in the early morning, decreas-
ing radical production rate in the mid-morning, followed by
a local maximum radical production rate around solar noon
have been observed during individual days in Milan and Pab-
sthum.

In Mexico City, we did not observe a symmetric radi-
cal production rate around solar noon; neither did we ob-
serve a dip in mid-morning. Rather, the peak of new radical
production is systematically shifted towards mid-morning,
i.e., around 10:00 a.m. or three hours before solar noon (see
Fig. 1). It is sustained at this high level until pollution is

efficiently exported from the MCMA. The absence of both a morning peak and a mid-morning dip in the radical production rate is attributed to the particularly high rate from secondary sources (all formed as a result of photochemical processing of pollutants): photolysis of HCHO, O_3, and other OVOCs in sum contribute about 75% of the radical production rate around 11:00 a.m., and 85% around 01:00 p.m. In other words, whatever radical source starts the processing of pollutants gets amplified by further radical production from secondary pollutants; the surrounding mountains trap secondary pollutants within the basin during mid-morning. Results from the MILAGRO/MCMA-2006 campaign (Dusanter et al., 2009; Molina et al., 2010) are generally consistent with our earlier findings. Our analysis highlights two phenomena: (1) the importance of radical sources that start the photochemical processing in the early morning; and (2) the non-linear feedbacks between meteorology (i.e., pollution export) and photochemical activity in the MCMA. These feedbacks have not been previously quantified at the radical level (i.e., radical production rates).

3.6.2 Absolute radical source strength

The overall radical production rate during MCMA-2003, as well as during the MILAGRO/MCMA-2006 field campaign (Dusanter et al., 2009) tends to be higher than in other urban environments, and on a routine basis is comparable to that found during a photochemical smog episode in Los Angeles in 1993 (Griffin et al., 2004). The radical production rate averaged over a 4-h time window centred near its peak is about 1.7 times higher than in Milan, 2 times that observed in Birmingham during summertime, 2.7 times that in Chelmsford, and 3 times higher than in Birmingham during wintertime. It is 3.3 times higher than in NYC and Nashville, 3.5 times higher than in Pabsthum, and 7–10 times than in rural environments. This comparison highlights the unique chemical activity of the Mexico City atmosphere.

Furthermore, the 24-h average HO_x radical production rate in the upper troposphere – 2.3×10^4 molec cm^{-3} s^{-1} (Singh et al., 1995; Arnold et al., 2004) – is two to three orders of magnitude lower than in the MCMA. Recently, higher than expected concentrations of oxygenated hydrocarbons have been measured in the free troposphere (Kwan et al., 2006). Interestingly, new HO_x production rates from CH_3CHO and CH_3COCH_3 in Mexico City are comparable to those in the free troposphere, about 5×10^5 and 10^4 molec cm^{-3} s^{-1} respectively (11 km height, solar zenith angle SZA=15 degrees, [CH_3CHO]=200 pptv, [CH_3COCH_3]=500 pptv). While O_3 or HCHO photolysis are important radical sources in both of these very different compartments of the atmosphere, the higher-than-expected concentrations of CH_3CHO in the free troposphere coupled with faster photolysis at higher altitude lead to HO_x production rates that compare or even exceed that from O_3 or HCHO photolysis, emphasizing the role of other radical sources than ozone at high altitude (Frost et al.,
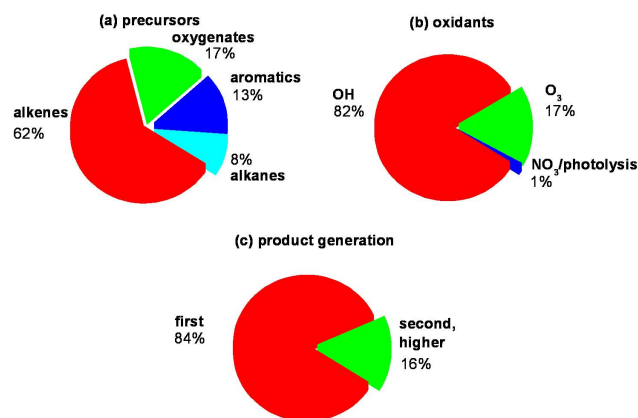

Fig. 6. Source apportionment of photochemical HCHO production. **(a)** The precursors of HCHO are separated by VOC class. **(b)** The effect of different oxidants is assessed. **(c)** The time scale of HCHO production is assessed in terms of oxidation step. An overwhelming majority of HCHO is formed as a first generation oxidation product from VOC oxidation; HCHO formation as second- and higher generation oxidation products makes only a minor contribution.

1999). The relevance of the polluted urban atmosphere as a source for oxidized hydrocarbons is expected to increase in the future.

3.6.3 Relative importance of different radical sources

The average daytime contribution to radical production rates from different sources in the MCMA is compared to other urban influenced environments in Table 2. While OVOC appear to be the most important radical source, the relative importance of other sources is fairly homogeneous (see also Table 1, and Sects. 3.1 and 3.7). This is different from previously studied atmospheres, in which typically one radical source dominates: HONO in NYC; HCHO in Milan; O_3 in the South Coast Air Basin in California (2010 scenario), and in Nashville, O_3/alkene reactions in Birmingham during wintertime, secondary OVOC in the South Coast Air Basin (1993 scenario), and in Birmingham and Chelmsford during summertime. Downwind of Berlin, in Pabsthum, O_3 and HCHO photolysis are both particularly important. Despite the considerable variability among different urban polluted, and between urban and rural atmospheres, some generalizations can be drawn.

HONO photolysis

We have included HONO among the radical sources in Tables 1 and 2, neglecting the fact that throughout most of the day a significant portion of HONO appears to be a radical reservoir instead of a radical source in the MCMA. At 09:00 a.m. virtually all HONO is accounted as PSS-HONO; dark HONO sources do not contribute significantly to the HONO production rate at that time. In the later morning and

Table 2. Comparison of the relative importance of radical sources in Mexico City with other urban and rural atmospheres (daytime average HO_x radical production rates).

	HCHO Phot.	HONO Phot.	O_3 Phot.	O_3/ alkenes	others	References
Rural boundary layer						
Pinnacle State Park, NY, USA	14	18	44	n.n.	25[a]	(Zhou et al., 2002)
Forest near Julich, GER	25	27	23	6	20[a]	(Kleffmann et al., 2005)
Hohenpreissenberg, GER	14	32	30	n.n.	25[a]	(Acker et al., 2006)
Urban boundary layer						
California South Coast Air Basin, USA:						(Griffin et al., 2004)
Central Los Angeles – 1993	21	11	31	6	31[e]	
Central Los Angeles – 2010	13	8	49	2	28[e]	
Azousa – 1993	17	6	28	6	43[e]	
Azousa – 2010	12	4	47	3	34[e]	
Riverside – 1993	14	4	32	3	47[e]	
Riverside – 2010	11	4	46	2	37[e]	
Milan, Italy	34	16	20	8	20[a]	(Alicke et al., 2002)
Nashville, TN, USA	29	8	47	0.2	20[a]	(Martinez et al., 2003)
Pabstum (near Berlin), GER	37	17	39	6	2[b]	(Alicke et al., 2003)
New York City, NY, USA	8	56	13	10	13[c]	(Ren et al., 2003)
Birmingham, UK (summer)	8	7	6	25	54[d]	(Emmerson et al., 2005)
Birmingham, UK (winter)	1	15	0.5	59	26[d]	
Chelmsford (near London), UK	6	10	14	20	50[d]	(Emmerson et al., 2007)
Mexico City, MEX – 2006	24	34	6	19	17[c]	(Dusanter et al., 2009)
Mexico City, MEX – 2003	19	12	19	12	38[d]	This work

[a] no number; value assumed for normalization and comparison purposes;
[b] only selected carbonyls measured; lower limit number;
[c] estimated using RACM;
[d] estimated using MCMv3.1 (mostly photolysis of OVOC);
[e] estimated using CIT air quality model (mostly photolysis of OVOC).

afternoon, the contribution from HONO to the overall radical production was low during MCMA-2003. Different results were obtained for HONO during the MILAGRO/MCMA-2006 field campaign, where in another part of town HONO was found to be tendentially higher, and much higher in episodes (Dusanter et al., 2009). During some episodes daytime HONO was significant, and during those episodes the contribution from daytime HONO can have a significant impact on the overall radical production (Li et al., 2010). However, results from MCMA-2003 and MILAGRO/MCMA-2006 show consistently that daytime HONO is not a routine occurrence in the MCMA, and the cause and frequency at which daytime HONO episodes occur are currently not well established.

Recently, significant daytime HONO concentrations in rural and forested environments indicate the presence of additional daytime HONO sources that are up to 64 times greater than the night time sources, and comparable to other sources like HCHO and O_3-photolysis (Zhou et al., 2002; Kleffmann et al., 2005; Acker et al., 2006). The only laboratory study that could thus far present convincing evidence

for atmospheric relevance is that by Stemmler et al. (2006). This photo-induced HONO source strength contributes about 0.3% to the ΣOH_{new} sources in the MCMA. Even a ten-fold increase in surface area (which in Mexico City is mostly due to abundant aerosol surface area, and only to a lesser extent due to vertical building surfaces) would make an insignificant contribution ($\sim$3%) to the overall noontime radical production rate here. Our observations are incompatible with findings in NYC (Ren et al., 2003), where HONO measurements with a wet-chemical technique (scrubbed derivatization HPLC) suggest high noontime radical production rates (about 10^7 molec cm^{-3} s^{-1}, or ten times the likely estimate, and twice the upper limit set by our measurements) corresponding to about 300 pptv of HONO. These high daytime HONO concentrations are directly observable with currently available spectroscopic techniques; they certainly should have been observable with our instruments, and were observed during certain episodes with similar instruments during the MILAGRO field campaign. Strong differences in the relative importance of HONO as a radical source seem to exist in different polluted urban environments even within a

city. Between NYC and the MCMA, differences exist in the types of available surface areas, the availability of sunlight in street-canyons, the vertical mixing-height and horizontal dispersion of pollutants. A direct confirmation of the HONO levels in NYC remains desirable. It is further noteworthy that our study identifies that secondary OVOC contribute about equal to radical production than HONO already shortly after sunrise.

HCHO-photolysis

The contribution from this source is highly variable. Compared to other urban environments, it is lower in the MCMA than downwind of Milan, Berlin and Nashville, but higher than in NYC, Birmingham and downwind of London. HCHO is an important radical source in the MCMA. About 70% of the average daytime radical production rate from HCHO is attributed to HCHO that forms from secondary sources (hydrocarbon photochemistry) (Garcia et al., 2006; Lei et al., 2009).

HCHO is emitted in significant amounts as part of vehicle exhaust in the MCMA (Zavala et al., 2006; Garcia et al., 2006). Conversely, targeted reductions of primary HCHO sources present an opportunity to slow down the rate of hydrocarbon oxidation. While primary HCHO only accounts for about 30% of the average daytime radical production rate from HCHO-photolysis, the contribution peaks at around 09:00 a.m., when the net-radical production rate from other sources is either no longer (HONO), or not yet (O_3) efficient. Primary HCHO sources contribute about 10% of the overall net-production of radicals before 10:00 a.m., and contribute significantly to the formation of those secondary species which sustain the exceptionally high ΣOH_{new} in the mid-morning. Reductions in primary HCHO sources can thus be expected to yield additional benefits from reducing the production rate of secondary species. Such amplification of benefits may however be out-weighed by parameters such as cycling chain length (Sheehy et al., 2010), which is highest in the early morning hours and decreasing towards the mid-morning, when primary HCHO contributes most to ΣOH_{new}. From a radical source perspective, the potential benefits of targeted primary HCHO reductions to reduce peak concentrations of secondary species like O_3 and SOA warrant future investigation. It is important that future research on this subject includes the development of models that adequately represent radical sources other than HCHO.

O_3-photolysis

The contribution from this source exceeds 30% only in semi-polluted and rural environments; it is generally below or close to 20% in more polluted environments, like Milan, NYC, and – interestingly – the MCMA. Despite frequent O_3 concentrations that exceed 100 ppbv in the MCMA, its 2220 m elevation above sea level, and tropical latitude, the daily average contribution from O_3 photolysis is not higher than that observed in other polluted atmospheres. This reflects efficient venting of the MCMA during afternoons (de Foy et al., 2006), and the abundance of other radical sources. The moderate contribution from O_3 photolysis in the urban atmosphere also means that any correlation of OH radical concentrations with J_{O_3} is rather a reflection of the fact that 85% of radical production is light-induced. Any such correlation should not be mistaken as evidence that O_3 indeed controls OH radical concentrations in the urban atmosphere.

O_3/alkene reactions

A markedly different contribution from O_3/alkene sources is observed compared to previous studies. Alkenes directly contribute to ΣOH_{new} by reacting with ozone. They contribute further indirectly to ΣOH_{new} as the oxidation of alkenes by OH as the predominant source for photochemical HCHO in Mexico City (see Sect. 3.5); photochemical sources are also the predominant source of ambient HCHO during the day (Garcia et al., 2006). In addition, O_3/alkene reactions essentially can explain most of the OH radical observations at night (see Fig. 3 in Sheehy et al., 2010), leading to the nighttime accumulation of secondary pollutants that produce radicals from secondary OVOC photolysis in the early morning hours. Further, the storage of nighttime OH-radicals in the form of PSS-HONO makes an important contribution to morning HONO levels. Photolysis of PSS-HONO, other OVOC and O_3/alkene reactions in sum are responsible for about 75% of the radical production rate one hour after sunrise. Notably, the three studies that employed a detailed chemical mechanism to study radical sources (Emmerson et al., 2005, 2007; this work) yield the highest estimates for the contribution from O_3/alkene reactions; lumped chemical codes seem to give lower estimates of O_3/alkene sources (see Table 2). O_3/alkene reactions make an important radical source during winter in Birmingham (Emmerson et al., 2005). The combined radical production rate attributable to alkene reactions exceeds that from any other source in the early morning in Mexico City. Notably, in the MCMA, the sum of the direct and indirect contributions of O_3/alkene reactions to ΣOH_{new} (on average about 30%) is at least five times higher compared to the relative abundance of alkenes on a ppbC basis (i.e., 3–6% ppbC at CENICA; see Velasco et al., 2007).

Photolysis of secondary OVOC

Most studies do not account for the radical production from the photolysis of OVOC other than HCHO. We find that OVOC photolysis other than HCHO accounts for 27% of the radical production about 1 h after sunrise, and this fraction increases to about 35% by 11:00 a.m. OVOC other than HCHO contribute about one third to the 12-h average daytime radical production rate during MCMA-2003.

The summed radical production of several hundred OVOC species is larger than the radical production from HCHO. There are only three other studies available that assessed the relative importance of OVOC; two used a similar approach to the work presented here (Emmerson et al., 2005, 2007), and another used a 3-dimensional chemical transport model (Griffin et al., 2004). These studies also found a large contribution of OVOC, independent of the season. It should be noted that previous 1-dimensional box-model studies did not take active precautions to account for the accumulation of secondary pollutants (N. Carslaw, personal communication, 2007), and allowed OVOC concentrations to reach a balance between photochemical production and sink reactions (quasi steady-state). If pollution export from the MCMA was neglected in our study, about 2–3 times higher contribution from OVOC is predicted by our model. However, our study shows that OVOC make a significant contribution also if dilution is taken into account. We conclude that OVOC are an important radical source in the early morning (nighttime accumulation) and indeed throughout the day in the MCMA. Further we conclude that pollution export from the MCMA lowers radical production rates inside the basin. OVOC photolysis is a major radical source also in the urban outflow from the MCMA (Apel et al., 2010).

Photolysis of ClNO$_2$

In Sect. 3.3.3 we estimated that heterogeneous N$_2$O$_5$ uptake to chloride containing aerosols can probably explain $\sim$10–15% of the observed O$_x$ loss at night, and leads to the accumulation of 2–3 ppb of ClNO$_2$ in the early morning. The photolysis of ClNO$_2$ forms Cl radicals, which efficiently react with VOCs and OVOCs to form RO$_2$ radicals in Mexico City (Cl addition is expected to be a minor pathway). We calculated J-values for ClNO$_2$ from our spectroradiometer data, assuming a unity quantum yield for Cl radical production, and the absorption cross-section from Sander et al. (2006). Typical J(ClNO$_2$) values during MCMA-2003 are $5\times10^{-5}\,\text{s}^{-1}$ at 07:00 a.m., $5\times10^{-4}\,\text{s}^{-1}$ at 09:00 a.m., and peak values are $\sim$9$\times10^{-4}\,\text{s}^{-1}$ around solar noon. Assuming 2 ppb ClNO$_2$, and $J(\text{ClNO}_2)=6\times10^{-4}\,\text{s}^{-1}$, the rate of Cl and thus RO$_2$ radical formation is estimated to be $2.3\times10^7\,\text{molec cm}^{-3}\,\text{s}^{-1}$. Based on this estimate, ClNO$_2$ photolysis adds 50% to the presently accounted RO$_2$ source, and corresponds to an extra 13% of ΣOH$_\text{new}$ under midmorning conditions, and $\sim$15% at 07:00 a.m. Despite the abundance of other radical sources in the MCMA, ClNO$_2$ photolysis seems to be relevant. A direct detection of ClNO$_2$ is therefore desirable.

Excited NO$_2$ reaction with water

If indeed operative, this reaction is not a significant source for OH radicals in the MCMA ($\sim$2% on the 12-h daytime average radical production rate, see Table 1).

3.7 Implications for Mexico City air quality

The peak concentrations of secondary pollutants, such as O$_3$ have decreased in recent years in Mexico City (Molina and Molina, 2002). It is presently not clear whether this is the result of (1) reductions in hydrocarbon emissions (VOC sensitivity of O$_3$ production); (2) a delay in the formation of O$_3$ (NO$_x$ suppressed O$_3$ formation in the early morning); or (3) reductions in light intensity near ground as a result of increasing light-absorbing PM pollution; any combination is indeed possible. In any of these scenarios the formation of secondary pollutants is radical-limited. Figure 7 shows radical sources grouped into primary (emission related) and secondary (photochemistry related) radical sources. In light of the amplification of early morning sources by secondary pollutants, reactions of anthropogenic alkenes are found to be particularly important; a lower limit for the radical production rate related to alkenes (either directly or indirectly) is also included in Fig. 7. Reductions in VOC emissions (in particular alkenes) are expected to induce reductions in peak concentrations of secondary pollutants like O$_3$ or SOA in three ways: (1) by lowering the rate of VOC oxidation as a result of a lower VOC/NO$_x$ ratio (effect of a lower radical re-cycling efficiency); (2) by slowing down the formation of secondary pollutants (effect of a lower radical production rate during the day and at night); and (3) by delaying the onset of photochemical processing; peak concentrations of secondary pollutants are capped by pollution export from the MCMA (effect of reducing the time available to produce secondary pollutants), see Sect. 3.1. To our knowledge, only pathway (1) has previously been associated with VOC reductions, whereas pathways (2) and (3) reflect additional feedbacks that are demonstrated in this study.

In this context it is interesting to note that lower emission scenarios in Los Angeles (compare 2010 scenario in Griffin et al., 2004) yield lower total RO$_x$ production rates and a shift in the relative importance of individual pathways. An analysis of how different radical sources respond to changes in future emission scenarios is desirable also for Mexico City, where – for the above reasons – a strong coupling to VOC reductions can be expected.

4 Conclusions and outlook

A detailed chemical code has been constrained by an extensive set of observations to characterize radical sources in the MCMA. There are several conclusions from this study:

- The photolysis of secondary OVOC contributes about 47% to the RO$_x$ production on a 12-h daytime average basis. OVOC other than HCHO are an important radical source despite the fact that (1) photolysis quantum yields of most carbonyls are significantly below unity, and (2) efficient pollution export in the afternoon has
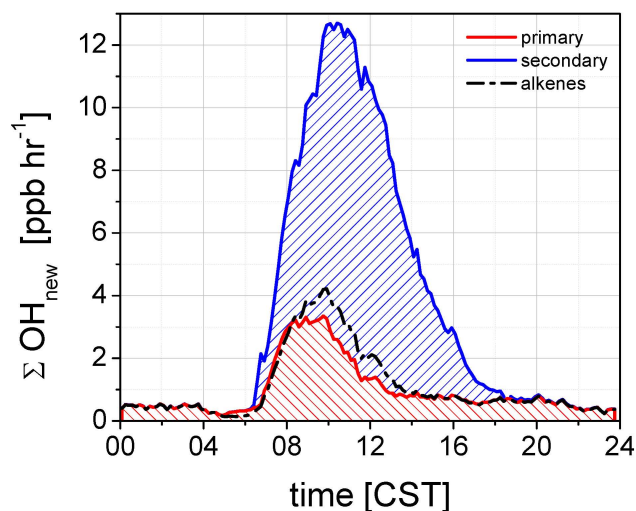
Fig. 7. The OH-equivalent radical production rate grouped by primary (emission related) vs. secondary (photochemistry related) sources. Primary sources are taken as the sum of O_3/alkenes, primary HCHO, the portion of PSS-HONO formed from primary radical sources, and alkene/NO_3 reactions. Secondary sources are taken as the photolysis of O_3, other HCHO, other OVOCs, the portion of PSS-HONO formed from secondary radical sources, unaccounted HONO, and further NO_3 reactions. The dashed-dot line represents a lower limit of the sum of primary and secondary ΣOH_{new} attributable to alkenes.

important feedbacks to lower radical production from secondary OVOC.

– Photo-induced formation of HONO contributes <3% to the radical production rate around noontime; furthermore HONO photolysis is found to be faster than expected. The contribution of HONO can vary by location and/or the meteorological conditions.

– $ClNO_2$ is likely a significant source of radicals in the MCMA; a direct detection of $ClNO_2$ is desirable.

– Alkene reactions are indirectly responsible for 75% of the radical production rate in the early morning, and 30% of OH reactivity throughout the day. The reactivity of alkenes adds secondary VOC that accumulate in the mid morning boundary layer. In the MCMA radical production does not follow the abundance of sunlight, but rather peaks already during mid-morning, (around 10:00 a.m.), mostly due to HCHO, O_3 and secondary OVOC photolysis, reflecting how the trapping of pollutants within the MCMA basin accelerates radical production rates and thus photochemistry. Due to this reduced solar zenith angle dependence, high radical production rates are expected year-round.

– Anthropogenic alkenes add little organic mass to SOA, but indirectly add to SOA by reacting to produce radicals for the processing of other SOA precursor VOCs.

This indirect SOA contribution of alkenes, i.e., to significantly add to oxidant fields, is likely to be much larger than their direct contribution to SOA mass.

– Three pathways are identified by which reductions in VOC emissions (in particular alkenes) benefit reductions in peak concentrations of secondary pollutants such as O_3 or SOA (see Sect. 3.7). The degree to which models could possibly capture the amplification of benefits from VOC reductions may depend on the level of detail represented in the respective underlying chemical codes. It remains to be verified whether important details such as radical production from O_3/alkene reactions are adequately represented in simplified chemical schemes that underlie the prediction of ozone and SOA in photochemical transport models.

– NO_3/VOC reactions are found to contribute little to radical production at roof-top-level, but contribute to the removal of furanone-type and phenol-type compounds during the day, and are expected to gain relative importance in the photochemical plume downwind of the MCMA. We present, to our knowledge, the first direct observation of NO_3 radicals in the urban center of a megacity.

– Future studies of radical sources in the polluted atmosphere need to take active measures to control the possibility of sampling artifacts with (1) the quantification of low O_3 levels (Dunlea et al., 2006) which may bias any results related to alkenes, accomplished here by the direct detection of O_3; and (2) alkene quantification and speciation by off-line analytical techniques (Atkinson et al., 1984; Jenkin et al., 2005), minimized here to the best possible degree by using a combination of an on-line FIS sensor, supplemented by VOC canister samples (Velasco et al., 2007). A direct confirmation of the alkene speciation by on-line techniques remains desirable in the MCMA.

– Finally, the current literature is biased towards observations made in air masses near the ground; little is known about how representative those observations are for the planetary boundary layer. Extrapolation from surface observations may not be straightforward due to the possibility of vertical gradients even during the day (Jobson et al., 2010); satellite data in turn provide only limited information about the vertical distribution of trace-gases. Future efforts need to assess the vertical distribution of relevant radical precursors in the MCMA and throughout the troposphere.

Edited by: C. E. Kolb

References

Acker, K., Moller, D., Wieprecht, W., Meixner, F. X., Bohn, B., Gilge, S., Plass-Dulmer, C., and Berresheim, H.: Strong daytime production of OH from HNO$_2$ at a rural mountain site, Geophys. Res. Lett., 33, L02809, doi:10.1029/2005GL024643, 2006.

Alicke, B., Geyer, A., Hofzumahaus, A., Holland, F., Konrad, S., Patz, H. W., Schafer, J., Stutz, J., Volz-Thomas, A., and Platt, U.: OH formation by HONO photolysis during the BERLIOZ experiment, J. Geophys. Res.-Atmos., 108, 8247–8263, 2003.

Alicke, B., Platt, U., and Stutz, J.: Impact of nitrous acid photolysis on the total hydroxyl radical budget during the Limitation of Oxidant Production/Pianura Padana Produzione di Ozono study in Milan, J. Geophys. Res.-Atmos., 107, 8196, doi:10.1029/2000JD000075, 2002.

Apel, E. C., Emmons, L. K., Karl, T., Flocke, F., Hills, A. J., Madronich, S., Lee-Taylor, J., Fried, A., Weibring, P., Walega, J., Richter, D., Tie, X., Mauldin, L., Campos, T., Weinheimer, A., Knapp, D., Sive, B., Kleinman, L., Springston, S., Zaveri, R., Ortega, J., Voss, P., Blake, D., Baker, A., Warneke, C., Welsh-Bon, D., de Gouw, J., Zheng, J., Zhang, R., Rudolph, J., Junkermann, W., and Riemer, D. D.: Chemical evolution of volatile organic compounds in the outflow of the Mexico City Metropolitan area, Atmos. Chem. Phys., 10, 2353–2375, doi:10.5194/acp-10-2353-2010, 2010.

Arens, F., Gutzwiller, L., Baltensperger, U., Gaggeler, H. W., and Ammann, M.: Heterogeneous reaction of NO$_2$ on diesel soot particles, Environ. Sci. Technol., 35, 2191–2199, 2001.

Arnold, S. R., Chipperfield, M. P., Blitz, M. A., Heard, D. E., and Pilling, M. J.: Photodissociation of acetone: Atmospheric implications of temperature-dependent quantum yields, Geophys. Res. Lett., 31, L07110, doi:10.1029/2003GL019099, 2004.

Arriaga-Colina, J. L., West, J. J., Sosa, G., Escalona, S. S., Ordunez, R. M., and Cervantes, A. D. M.: Measurements of VOCs in Mexico City (1992–2001) and evaluation of VOCs and CO in the emissions inventory, Atmos. Environ., 38, 2523–2533, 2004.

Atkinson, R., Aschmann, S. M., Winer, A. M., and Pitts, J. N.: Gas-Phase Reaction of NO$_2$ with Alkenes and Dialkenes, Int. J. Chem. Kinet., 16, 697–706, 1984.

Bass, A. M. and Paur, R. J.: Uv Absorption Cross-Sections for Ozone – the Temperature-Dependence, J. Photochem., 17, p. 141, 1981.

Bell, M. L., McDermott, A., Zeger, S. L., Samet, J. M., and Dominici, F.: Ozone and short-term mortality in 95 US urban communities, 1987–2000, Jama-J. Am. Med. Assoc., 292, 2372–2378, 2004.

Behnke, W., George, C., Scheer, V., and Zetzsch, C.: Production and decay of ClNO2, from the reaction of gaseous N$_2$O$_5$ with NaCl solution: Bulk and aerosol experiments, J. Geophys. Res., 102, 3795–3804, 1997.

Bernath, P., Carleer, M., Fally, S., Jenouvrier, A., Vandaele, A. C., Hermans, C., Merienne, M. F., and Colin, R.: The Wulf bands of oxygen, Chem. Phys. Lett., 297, 293–299, 1998.

Bloss, C., Wagner, V., Bonzanini, A., Jenkin, M. E., Wirtz, K., Martin-Reviejo, M., and Pilling, M. J.: Evaluation of detailed aromatic mechanisms (MCMv3 and MCMv3.1) against environmental chamber data, Atmos. Chem. Phys., 5, 623–639, doi:10.5194/acp-5-623-2005, 2005a.

Bloss, C., Wagner, V., Jenkin, M. E., Volkamer, R., Bloss, W. J., Lee, J. D., Heard, D. E., Wirtz, K., Martin-Reviejo, M., Rea, G., Wenger, J. C., and Pilling, M. J.: Development of a detailed chemical mechanism (MCMv3.1) for the atmospheric oxidation of aromatic hydrocarbons, Atmos. Chem. Phys., 5, 641–664, doi:10.5194/acp-5-641-2005, 2005b.

Brown, S. S., Osthoff, H. D., Stark, H., Dube, W. P., Ryerson, T. B., Warneke, C., de Gouw, J. A., Wollny, A. G., Parrish, D. D., Fehsenfeld, F. C., and Ravishankara, A. R.: Aircraft observations of daytime NO3 and N$_2$O$_5$ and their implications for tropospheric chemistry, J. Photoch. Photobio. A, 176, 270–278, 2005.

Brown, S. S., Ryerson, T. B., Wollny, A. G., Brock, C. A., Peltier, R., Sullivan, A. P., Weber, R. J., Dube, W. P., Trainer, M., Meagher, J. F., Fehsenfeld, F. C., and Ravishankara, A. R.: Variability in nocturnal nitrogen oxide processing and its role in regional air quality, Science, 311, 67–70, 2006.

Cantrell, C. A., Davidson, J. A., Mcdaniel, A. H., Shetter, R. E., and Calvert, J. G.: Temperature-Dependent Formaldehyde Cross-Sections in the Near-Ultraviolet Spectral Region, J. Phys. Chem.-US, 94, 3902–3908, 1990.

Carter, W. P. L.: Environmental Chamber Studies of Ozone Formation Potentials of Volatile Organic Compounds, in: Environmental Simulation Chambers: Application to Atmospheric Chemical Processes, edited by:Rudzinski, K. and Barnes, I., Proceedings of the NATO Advanced Research Workshop, Zakopane, Poland 1–4 October, 2004, NATO Sciences Series, IV. Earth and Environmental Sciences. Vol. 62. Kluwer Publishing, Doortrecht, The Netherlands, 2005.

Davis, D. L., Bell, M. L., and Fletcher, T.: A look back at the London smog of 1952 and the half century since, Environ. Health Persp., 110, A734–A735, 2002.

de Foy, B., Varela, J. R., Molina, L. T., and Molina, M. J.: Rapid ventilation of the Mexico City basin and regional fate of the urban plume, Atmos. Chem. Phys., 6, 2321–2335, doi:10.5194/acp-6-2321-2006, 2006.

Donaldson, D. J., Frost, G. J., Rosenlof, K. H., Tuck, A. F., and Vaida, V.: Atmospheric radical production by excitation of vibrational overtones via absorption of visible light, Geophys. Res. Lett., 24, 2651–2654, 1997.

Dunlea, E. J., Herndon, S. C., Nelson, D. D., Volkamer, R. M., Lamb, B. K., Allwine, E. J., Grutter, M., Ramos Villegas, C. R., Marquez, C., Blanco, S., Cardenas, B., Kolb, C. E., Molina, L. T., and Molina, M. J.: Technical note: Evaluation of standard ultraviolet absorption ozone monitors in a polluted urban environment, Atmos. Chem. Phys., 6, 3163–3180, doi:10.5194/acp-6-3163-2006, 2006.

Dusanter, S., Vimal, D., Stevens, P. S., Volkamer, R., Molina, L.

T., Baker, A., Meinardi, S., Blake, D., Sheehy, P., Merten, A., Zhang, R., Zheng, J., Fortner, E. C., Junkermann, W., Dubey, M., Rahn, T., Eichinger, B., Lewandowski, P., Prueger, J., and Holder, H.: Measurements of OH and HO_2 concentrations during the MCMA-2006 field campaign – Part 2: Model comparison and radical budget, Atmos. Chem. Phys., 9, 6655–6675, doi:10.5194/acp-9-6655-2009, 2009.

Dzepina, K., Volkamer, R. M., Madronich, S., Tulet, P., Ulbrich, I. M., Zhang, Q., Cappa, C. D., Ziemann, P. J., and Jimenez, J. L.: Evaluation of recently-proposed secondary organic aerosol models for a case study in Mexico City, Atmos. Chem. Phys., 9, 5681–5709, doi:10.5194/acp-9-5681-2009, 2009.

Emmerson, K. M., Carslaw, N., and Pilling, M. J.: Urban atmospheric chemistry during the PUMA campaign 2: Radical budgets for OH, HO_2 and RO_2, J. Atmos. Chem., 52, 165–183, 2005.

Emmerson, K. M., Carslaw, N., Carslaw, D. C., Lee, J. D., McFiggans, G., Bloss, W. J., Gravestock, T., Heard, D. E., Hopkins, J., Ingham, T., Pilling, M. J., Smith, S. C., Jacob, M., and Monks, P. S.: Free radical modelling studies during the UK TORCH Campaign in Summer 2003, Atmos. Chem. Phys., 7, 167–181, doi:10.5194/acp-7-167-2007, 2007.

Fally, S., Vandaele, A. C., Carleer, M., Hermans, C., Jenouvrier, A., Merienne, M. F., Coquart, B., and Colin, R.: Fourier transform spectroscopy of the O-2 Herzberg bands. III. Absorption cross sections of the collision-induced bands and of the Herzberg continuum, J. Mol. Spectrosc., 204, 10–20, 2000.

Fayt, C. and van Roozendael, M.: WinDoas 2.1 – Software User Manual, Brussels: BIRA-IASB, 2001.

Finlayson-Pitts, B. J., Ezell, M. J., and Pitts Jr., J. N.: Formation of Chemically Active Chlorine Compounds by Reactions of Atmospheric NaCl Particles with Gaseous N_2O_5 and $ClONO_2$, Nature, 337, 241–244, doi:10.1038/337241a0, 1989.

Fuhrer, J. and Booker, F.: Ecological issues related to ozone: agricultural issues, Environ. Int., 29, 141–154, 2003.

Frost, G. J., Trainer, M., Mauldin, R. L., Eisele, F. L., Prevot, A. S. H., Flocke, S. J., Madronich, S., Kok, G., Schillawski, R. D., Baumgardner, D., and Bradshaw, J.: Photochemical modeling of OH levels during the first aerosol characterization experiment (ACE 1), J. Geophys. Res.-Atmos., 104, 16041–16052, 1999.

Garcia, A. R., Volkamer, R., Molina, L. T., Molina, M. J., Samuelson, J., Mellqvist, J., Galle, B., Herndon, S. C., and Kolb, C. E.: Separation of emitted and photochemical formaldehyde in Mexico City using a statistical analysis and a new pair of gas-phase tracers, Atmos. Chem. Phys., 6, 4545–4557, doi:10.5194/acp-6-4545-2006, 2006.

Geyer, A., Alicke, B., Ackermann, R., Martinez, M., Harder, H., Brune, W., de Carlo, P., Williams, E., Jobson, T., Hall, S., Shetter, R., and Stutz, J.: Direct observations of daytime NO3: Implications for urban boundary layer chemistry, J. Geophys. Res.-Atmos., 108, 4368, doi:10.1029/2002JD002967, 2003.

Gomer, T., Brauers, T., Heintz, F., Stutz, J., and Platt, U.: MFC User Manual, Version 1.98, Institut fuer Umweltphysik, University of Heidelberg, 1993.

Gregg, J. W., Jones, C. G., and Dawson, T. E.: Urbanization effects on tree growth in the vicinity of New York City, Nature, 424, 183–187, 2003.

Griffin, R. J.: Modeling the oxidative capacity of the atmosphere of the South Coast Air Basin of California. 2. HOx radical production, Environ. Sci. Technol. 38, 753–757, 2004.

Haagen-Smit, A. J., Darley, E. F., Zaitlin, M., Hull, H., and Nobel, W.: Investigation on injury to plants from air pollution in the Los Angeles area, Plant Physiol., 27, p. 18, 1951.

Hasson, A. S., Tyndall, G. S., and Orlando, J. J.: A product yield study of the reaction of HO2 radicals with ethyl peroxy (C2H5O2), acetyl peroxy (CH3C(O)O-2), and acetonyl peroxy (CH3C(O)CH2O2) radicals, J. Phys. Chem. A, 108, 5979–5989, 2004.

Health Effects Institute: Reanalysis of the Harvard Six Cities Study and the American Cancer Society Study of Particulate Air Pollution and Mortality: A Special Report of the Institute's Particle Epidemiology Reanalysis Project. Library of Congress Catalog Number for the HEI Report Series: WA 754 R432, Health Effects Institute, Cambridge, MA, 2000.

IPCC: A Report of Working Group I of the Intergovernmental Panel on Climate Change: Summary for Policymakers, online available at: http://www.ipcc.ch/, 2007.

Jauregui, E.: Mexico City's urban heat island revisited, Erdkunde, 47, 185–195, 1993.

Jenkin, M. E., Andersen, M. P. S., Hurley, M. D., Wallington, T. J., Taketani, F., and Matsumi, Y.: A kinetics and mechanistic study of the OH and NO2 initiated oxidation of cyclohexa-1,3-diene in the gas phase, Phys. Chem. Chem. Phys., 7, 1194–1204, 2005.

Jenkin, M. E., Saunders, S. M., Wagner, V., and Pilling, M. J.: Protocol for the development of the Master Chemical Mechanism, MCM v3 (Part B): tropospheric degradation of aromatic volatile organic compounds, Atmos. Chem. Phys., 3, 181–193, doi:10.5194/acp-3-181-2003, 2003.

Jenouvrier, A., Merienne, M. F., Coquart, B., Carleer, M., Fally, S., Vandaele, A. C., Hermans, C., and Colin, R.: Fourier transform spectroscopy of the O-2 Herzberg bands – I. Rotational analysis, J. Mol. Spectrosc., 198, 136–162, 1999.

Jobson, B. T., Volkamer, R. A., Velasco, E., Allwine, G., Westberg, H., Lamb, B. K., Alexander, M. L., Berkowitz, C. M., and Molina, L. T.: Comparison of aromatic hydrocarbon measurements made by PTR-MS, DOAS and GC-FID during the MCMA 2003 Field Experiment, Atmos. Chem. Phys., 10, 1989–2005, doi:10.5194/acp-10-1989-2010, 2010.

Kleffmann, J., Gavriloaiei, T., Hofzumahaus, A., Holland, F., Koppmann, R., Rupp, L., Schlosser, E., Siese, M., and Wahner, A.: Daytime formation of nitrous acid: A major source of OH radicals in a forest, Geophys. Res. Lett., 32, L05818, doi:10.1029/2005GL022524, 2005.

Kleffmann, J., Lorzer, J. C., Wiesen, P., Kern, C., Trick, S., Volkamer, R., Rodenas, M., and Wirtz, K.: Intercomparison of the DOAS and LOPAP techniques for the detection of nitrous acid (HONO), Atmos. Environ., 40, 3640–3652, 2006.

Kraus, A., Rohrer, F., and Hofzumahaus, A.: Intercomparison of NO2 photolysis frequency measurements by actinic flux spectroradiometry and chemical actinometry during JCOM97, Geophys. Res. Lett., 27, 1115–1118, 2000.

Kurtenbach, R., Ackermann, R., Becker, K. H., Geyer, A., Gomes, J. A. G., Lorzer, J. C., Platt, U., and Wiesen, P.: Verification of the contribution of vehicular traffic to the total NMVOC emissions in Germany and the importance of the NO_3 chemistry in the city air, J. Atmos. Chem., 42, 395–411, 2002.

Kwan, A. J., Crounse, J. D., Clarke, A. D., Shinozuka, Y., Anderson, B. E., Crawford, J. H., Avery, M. A., McNaughton, C. S., Brune, W. H., Singh, H. B., and Wennberg, P. O.:

On the flux of oxygenated volatile organic compounds from organic aerosol oxidation, Geophys. Res. Lett., 33, L15815, doi:10.1029/2006GL026144, 2006.

Lei, W., de Foy, B., Zavala, M., Volkamer, R., and Molina, L. T.: Characterizing ozone production in the Mexico City Metropolitan Area: a case study using a chemical transport model, Atmos. Chem. Phys., 7, 1347–1366, doi:10.5194/acp-7-1347-2007, 2007.

Lei, W., Zavala, M., de Foy, B., Volkamer, R., and Molina, L. T.: Characterizing ozone production and response under different meteorological conditions in Mexico City, Atmos. Chem. Phys., 8, 7571–7581, doi:10.5194/acp-8-7571-2008, 2008.

Lei, W., Zavala, M., de Foy, B., Volkamer, R., Molina, M. J., and Molina, L. T.: Impact of primary formaldehyde on air pollution in the Mexico City Metropolitan Area, Atmos. Chem. Phys., 9, 2607–2618, doi:10.5194/acp-9-2607-2009, 2009.

Li, G., Lei, W., Zavala, M., Volkamer, R., Dusanter, S., Stevens, P., and Molina, L. T.: Impacts of HONO sources on the photochemistry in Mexico City during the MCMA-2006/MILAGO Campaign, Atmos. Chem. Phys., 10, 6551–6567, doi:10.5194/acp-10-6551-2010, 2010.

Li, S. P., Matthews, J., and Sinha, A.: Atmospheric hydroxyl radical production from electronically excited NO_2 and H_2O, Science, 319, 1657–1660, 2008.

Martinez, M., Harder, H., Kovacs, T. A., Simpas, J. B., Bassis, J., Lesher, R., Brune, W. H., Frost, G. J., Williams, E. J., Stroud, C. A., Jobson, B. T., Roberts, J. M., Hall, S. R., Shetter, R. E., Wert, B., Fried, A., Alicke, B., Stutz, J., Young, V. L., White, A. B., and Zamora, R. J.: OH and HO_2 concentrations, sources, and loss rates during the Southern Oxidants Study in Nashville, Tennessee, summer 1999, J. Geophys. Res.-Atmos., 108, 4617–4633, 2003.

Merienne, M. F., Jenouvrier, A., Coquart, B., Carleer, M., Fally, S., Colin, R., Vandaele, A. C., and Hermans, C.: Fourier transform spectroscopy of the O-2 Herzberg bands – II. Band oscillator strengths and transition moments, J. Mol. Spectrosc., 202, 171–193, 2000.

Merienne, M. F., Jenouvrier, A., Coquart, B., Carleer, M., Fally, S., Colin, R., Vandaele, A. C., and Hermans, C.: Improved data set for the Herzberg band systems of O-16(2), J. Mol. Spectrosc., 207, 120–120, 2001.

Molina, L. T. and Molina, M. J.: Air Quality in the Mexico Megacity: An Integrated Assessment, Kluwer Academic Publishers, Dordrecht, The Netherlands, 105–136, 2002.

Molina, L. T., Kolb, C. E., de Foy, B., Lamb, B. K., Brune, W. H., Jimenez, J. L., Ramos-Villegas, R., Sarmiento, J., Paramo-Figueroa, V. H., Cardenas, B., Gutierrez-Avedoy, V., and Molina, M. J.: Air quality in North America's most populous city – overview of the MCMA-2003 campaign, Atmos. Chem. Phys., 7, 2447–2473, doi:10.5194/acp-7-2447-2007, 2007.

Molina, L. T., Madronich, S., Gaffney, J. S., Apel, E., de Foy, B., Fast, J., Ferrare, R., Herndon, S., Jimenez, J. L., Lamb, B., Osornio-Vargas, A. R., Russell, P., Schauer, J. J., Stevens, P. S., and Zavala, M.: An overview of the MILAGRO 2006 campaign: Mexico City emissions and their transport and transformation, Atmos. Chem. Phys. Discuss., 10, 7819–7983, doi:10.5194/acpd-10-7819-2010, 2010.

Nel, A.: Air Pollution-Related Illness: Effects of Particles, Science, 308, 804–806, 2005.

Oke, T. R., Spronken-Smith, R. A., Jauregui, E., and Grimmond, C. S. B.: The energy balance of central Mexico City during the dry season, Atmos. Environ., 33, 3919–3930, 1999.

Orphal, J.: A critical review of the absorption cross-sections of O_3 and NO_2 in the ultraviolet and visible, J. Photoch. Photobio. A, 157, 185–209, 2003.

PAPA, Public Health and Air Pollution in Asia (PAPA) Special Report 15: Health Effects of Outdoor Air Pollution in Developing Countries of Asia. Library of Congress Catalog Number for the HEI Report Series: WA 754 R432, Health Effects Institute, Cambridge, MA, 2004.

Platt, U.: Differential Optical Absorption Spectroscopy, in Monitoring by Spectroscopic Techniques, edited by M. W. Sigrist, Wiley & Sons, New York, 27–84, 1994.

Platt, U., Perner, D., Harris, G. W., Winer, A. M., and Pitts, J. N.: Observations of Nitrous-Acid in An Urban Atmosphere by Differential Optical-Absorption, Nature, 285, 312–314, 1980.

Pope, C. A., Burnett, R. T., Thun, M. J., Calle, E. E., Krewski, D., Ito, K., and Thurston, G. D.: Lung cancer, cardiopulmonary mortality, and long-term exposure to fine particulate air pollution, Jama-J. Am. Med. Assoc., 287, 1132–1141, 2002.

Ramanathan, V., Crutzen, P. J., Kiehl, J. T., and Rosenfeld, D.: Aerosols, Climate, and the Hydrological Cycle, Science, 294, 2119–2124, 2001.

Ramazan, K. A., Wingen, L. M., Miller, Y., Chaban, G. M., Gerber, R. B., Xantheas, S. S., and Finlayson-Pitts, B. J.: New experimental and theoretical approach to the heterogeneous hydrolysis of NO2: Key role of molecular nitric acid and its complexes, J. Phys. Chem. A, 110, 6886–6897, 2006.

Ren, X. R., Harder, H., Martinez, M., Lesher, R. L., Oliger, A., Simpas, J. B., Brune, W. H., Schwab, J. J., Demerjian, K. L., He, Y., Zhou, X. L., and Gao, H. G.: OH and HO_2 Chemistry in the urban atmosphere of New York City, Atmos. Environ., 37, 3639–3651, 2003.

Roberts, J. M., Osthoff, H. D., Brown, S. S., and Ravishankara, A. R.: N_2O_5 oxidizes chloride to Cl_2 in acidic atmospheric aerosol, Science, 321, p. 1059, 2008.

Robinson, A. L., Donahue, N. M., Shrivastava, M. K., Weitkamp, E. A., Sage, A. M., Grieshop, A. P., Lane, T. E., Pierce, J. R., and Pandis, S. N.: Rethinking organic aerosols: Semivolatile emissions and photochemical aging, Science, 315, 1259–1262, 2007.

Ruiz-Suarez, L. G., Castro, T., Mar, B., Ruiz-Santoyo, M. E., and Cruz, X.: Do We Need An Ad Hoc Chemical Mechanism for Mexico-City Photochemical Smog, Atmos. Environ. A-Gen., 27, 405–425, 1993.

Salcedo, D., Onasch, T. B., Dzepina, K., Canagaratna, M. R., Zhang, Q., Huffman, J. A., DeCarlo, P. F., Jayne, J. T., Mortimer, P., Worsnop, D. R., Kolb, C. E., Johnson, K. S., Zuberi, B., Marr, L. C., Volkamer, R., Molina, L. T., Molina, M. J., Cardenas, B., Bernabé, R. M., Márquez, C., Gaffney, J. S., Marley, N. A., Laskin, A., Shutthanandan, V., Xie, Y., Brune, W., Lesher, R., Shirley, T., and Jimenez, J. L.: Characterization of ambient aerosols in Mexico City during the MCMA-2003 campaign with Aerosol Mass Spectrometry: results from the CENICA Supersite, Atmos. Chem. Phys., 6, 925–946, doi:10.5194/acp-6-925-2006, 2006.

Sander, S. P., Friedl, R. R., Golden, D. M., Kurylo, M. J., Moortgat, G. K., Keller-Rudeck, H., Wine, P. H., Ravishankara, A. R., Kolb, C. E., Molina, M. J., Finlayson-Pitts, B. J., Huie, R. E.,

and Orkin, R. L.: Chemical Kinetics and Photochemical Data for Use in Atmospheric Studies Evaluation Number 15, JPL Publication, 06-2, 1–522, 2006.

Saunders, S. M., Jenkin, M. E., Derwent, R. G., and Pilling, M. J.: Protocol for the development of the Master Chemical Mechanism, MCM v3 (Part A): tropospheric degradation of non-aromatic volatile organic compounds, Atmos. Chem. Phys., 3, 161–180, doi:10.5194/acp-3-161-2003, 2003.

Sheehy, P. M., Volkamer, R., Molina, L. T., and Molina, M. J.: Oxidative capacity of the Mexico City atmosphere – Part 2: A RO_x radical cycling perspective, Atmos. Chem. Phys., 10, 6993–7008, doi:10.5194/acp-10-6993-2010, 2010.

Shirley, T. R., Brune, W. H., Ren, X., Mao, J., Lesher, R., Cardenas, B., Volkamer, R., Molina, L. T., Molina, M. J., Lamb, B., Velasco, E., Jobson, T., and Alexander, M.: Atmospheric oxidation in the Mexico City Metropolitan Area (MCMA) during April 2003, Atmos. Chem. Phys., 6, 2753–2765, doi:10.5194/acp-6-2753-2006, 2006.

Singh, H. B., Kanakidou, M., Crutzen, P. J., and Jacob, D. J.: High-Concentrations and Photochemical Fate of Oxygenated Hydrocarbons in the Global Troposphere, Nature, 378, 50–54, 1995.

Stemmler, K., Ammann, M., Donders, C., Kleffmann, J., and George, C.: Photosensitized reduction of nitrogen dioxide on humic acid as a source of nitrous acid, Nature, 440, 195–198, 2006.

Stephens, S., Madronich, S., Wu, F., Olson, J. B., Ramos, R., Retama, A., and Muñoz, R.: Weekly patterns of México City's surface concentrations of CO, NO_x, PM_{10} and O_3 during 1986–2007, Atmos. Chem. Phys., 8, 5313–5325, doi:10.5194/acp-8-5313-2008, 2008.

Stutz, J., Alicke, B., Ackermann, R., Geyer, A., Wang, S. H., White, A. B., Williams, E. J., Spicer, C. W., and Fast, J. D.: Relative humidity dependence of HONO chemistry in urban areas, J. Geophys. Res.-Atmos., 109, D03307, doi:10.1029/2003JD004135, 2004.

Stutz, J., Kim, E. S., Platt, U., Bruno, P., Perrino, C., and Febo, A.: UV-visible absorption cross sections of nitrous acid, J. Geophys. Res.-Atmos., 105, 14585–14592, 2000.

Vandaele, A. C., Simon, T., Giolmont, J., Carleer, C., and Colin, R.: SO_2 absorption cross section measurement in the UV using fourier transform spectrometer, J. Geophys. Res., 99, 25599–25605, 1994.

Velasco, E., Lamb, B., Westberg, H., Allwine, E., Sosa, G., Arriaga-Colina, J. L., Jobson, B. T., Alexander, M. L., Prazeller, P., Knighton, W. B., Rogers, T. M., Grutter, M., Herndon, S. C., Kolb, C. E., Zavala, M., de Foy, B., Volkamer, R., Molina, L. T., and Molina, M. J.: Distribution, magnitudes, reactivities, ratios and diurnal patterns of volatile organic compounds in the Valley of Mexico during the MCMA 2002 & 2003 field campaigns, Atmos. Chem. Phys., 7, 329–353, doi:10.5194/acp-7-329-2007, 2007.

Volkamer, R., Etzkorn, T., Geyer, A., and Platt, U.: Correction of the oxygen interference with UV spectroscopic (DOAS) measurements of monocyclic aromatic hydrocarbons in the atmosphere, Atmos. Environ., 32, 3731–3747, 1998.

Volkamer, R., Platt, U., and Wirtz, K.: Primary and Secondary Glyoxal Formation from Aromatics: Experimental Evidence for the Bicycloalkyl-Radical Pathway from Benzene, Toluene, and p-Xylene, J. Phys. Chem. A, 105, 7865–7874, 2001.

Volkamer, R., Molina, L. T., Molina, M. J., Shirley, T., and Brune, W. H.: DOAS measurement of glyoxal as an indicator for fast VOC chemistry in urban air, Geophys. Res. Lett., 32, L08806, doi:10.1029/2005GL022616, 2005a.

Volkamer, R., Spietz, P., Burrows, J. P., and Platt, U.: High-resolution absorption cross-section of Glyoxal in the UV/vis and IR spectral ranges, J. Photoch. Photobio. A, 172, 35–46, 2005b.

Volkamer, R., Jimenez, J. L., San Martini, F., Dzepina, K., Zhang, Q., Salcedo, D., Molina, L. T., Worsnop, D. R., and Molina, M. J.: Secondary organic aerosol formation from anthropogenic air pollution: Rapid and higher than expected, Geophys. Res. Lett., 33, L17811, doi:10.1029/2006GL026899, 2006.

von Friedeburg, C., Wagner, T., Geyer, A., Kaiser, N., Vogel, B., Vogel, H., and Platt, U.: Derivation of tropospheric NO_3 profiles using off-axis differential optical absorption spectroscopy measurements during sunrise and comparison with simulations, J. Geophys. Res.-Atmos., 107, 4168, doi:10.1029/2001JD000481, 2002.

Wall, K. J., Schiller, C. L., and Harris, G. W.: Measurements of the HONO photodissociation constant, J. Atmos. Chem., 55, 31–54, 2006.

West, J. J., Zavala, M. A., Molina, L. T., Molina, M. J., San Martini, F., McRae, G. J., Sosa-Iglesias, G., and Arriaga-Colina, J. L.: Modeling ozone photochemistry and evaluation of hydrocarbon emissions in the Mexico City metropolitan area, J. Geophys. Res.-Atmos., 109, D19312, doi:10.1029/2004JD004614, 2004.

Witonsky, S. K., Canagaratna, M. R., Coy, S. L., Steinfeld, J. I., Field, R. W., and Kachanov, A. A.: The 3 nu(1) overtone band of trans-nitrous acid: Rotational and perturbation analysis and absolute intensity, J. Chem. Phys., 115, 3134–3143, 2001.

Zavala, M., Herndon, S. C., Slott, R. S., Dunlea, E. J., Marr, L. C., Shorter, J. H., Zahniser, M., Knighton, W. B., Rogers, T. M., Kolb, C. E., Molina, L. T., and Molina, M. J.: Characterization of on-road vehicle emissions in the Mexico City Metropolitan Area using a mobile laboratory in chase and fleet average measurement modes during the MCMA-2003 field campaign, Atmos. Chem. Phys., 6, 5129–5142, doi:10.5194/acp-6-5129-2006, 2006.

Zhang, Q., Jimenez, J. L., Canagaratna, M. R., Allan, J. D., Coe, H., Ulbrich, I., Alfarra, M. R., Takami, A., Middlebrook, A. M., Sun, Y. L., Dzepina, K., Dunlea, E., Docherty, K., deCarlo, P. F., Salcedo, D., Onasch, T., Jayne, J. T., Miyoshi, T., Shimono, A., Hatakeyama, S., Takegawa, N., Kondo, Y., Schneider, J., Drewnick, F., Borrmann, S., Weimer, S., Demerjian, K., Williams, P., Bower, K., Bahreini, R., Cottrell, L., Griffin, R. J., Rautiainen, J., Sun, J. Y., Zhang, Y. M., and Worsnop, D. R.: Ubiquity and dominance of oxygenated species in organic aerosols in anthropogenically-influenced Northern Hemisphere midlatitudes, Geophys. Res. Lett., 34, L13801, doi:10.1029/2007GL029979, 2007.

Zhou, X. L., Civerolo, K., Dai, H. P., Huang, G., Schwab, J., and Demerjian, K.: Summertime nitrous acid chemistry in the atmospheric boundary layer at a rural site in New York State, J. Geophys. Res.-Atmos., 107, 4590, doi:10.1029/2001JD001539, 2002.